Lineage-specific proteome remodeling of diverse lung cancer cells by targeted epigenetic inhibitors

Chuwei Lin[1], Catherine Sniezek[1], Ross M Giglio[2], Rashmi Karki[3], Christopher McGann[1], Benjamin A. Garcia[3], Jose L McFaline-Figeroa[2], Devin K. Schweppe[1, *]

[1] University of Washington, Seattle, WA 98105, USA

[2] Columbia University, New York, NY 10027, USA

[3] Washington University School of Medicine, St. Louis, MO 63110, USA

*Email: dkschwep@uw.edu

Abstract

Epigenetic inhibitors exhibit powerful antiproliferative and anticancer activities. However, cellular responses to small-molecule epigenetic inhibition are heterogenous and dependent on factors such as the genetic background, metabolic state, and on-/off-target engagement of individual small-molecule drugs. To determine the mechanisms that drive these heterogeneous cellular responses, we quantified chromatin, proteome, and transcriptome remodeling due to histone deacetylase inhibitor (HDACi) -treated cells derived from diverse genetic backgrounds. We utilized high-throughput sample multiplexed proteomics and integrated intelligent data acquisition methods to map proteomes of cancer cell lines in response to HDACi. We determined cell type-specific and ubiquitous cellular responses based on the quantification of 10,621 total proteins. We then established how coordinated remodeling of the proteome, transcriptome and chromatin state of HDACi treated cancer cells revealed convergent (JUN, MAP2K3, CDKN1A) and divergent (CCND3, ASF1B, BRD7) molecular phenotypes. HDACi-regulated proteins differ greatly across cell lines owing to heterogeneous molecular states of these cell lines. Finally, we demonstrated that HDACi treatment drove a highly cell-type specific response that may in part be explained by cell line-specific off-target drug engagement.

Introduction

Regulation of gene expression is essential to maintain cell homeostasis. In eukaryotic cells, histones are essential for these processes as they regulate RNA polymerase access to chromatin and other transcription factors to bind their target genes, by packaging chromatin. Histone acetylation is an essential post-translational modification for this process. Because of this, the histone acetylation/deacetylation balance in cells is key to maintaining the cellular chromatin state. Dysregulation of this state has been associated with poor prognosis in gastric cancer (Sudo et al., 2011; Weichert, Röske, et al., 2008), ovarian cancer (Hayashi et al., 2010), and lung cancer (Jung, Noh, Kim, Eun, Bae, Chang, et al., 2012; Minamiya et al., 2011). Thus, due to histone deacetylases' (HDACs') relationship with lung carcinogenesis, HDAC inhibition has been a potential target for therapeutic intervention for many years (Y. Li & Seto, 2016).

Histone acetyl transferases modify histones to drive gene expression and HDACs remove acetyl groups from histones to repress gene transcription (Inoue & Fujimoto, 1969). To date, there have been 18 HDACs identified in humans which are divided into four classes based on their structures (Seto & Yoshida, 2014). Class I includes HDAC1, 2, 3 and 8, which are found in the

nucleus. Class II includes HDAC4, 5, 6, 7, 9 and 10, which shuttle between the nucleus and cytoplasm. Class III requires NAD+ for their enzyme activity. HDAC11 is the only one classified as Class IV that shares similarity with both Class I and Class II. As critical regulators of gene expression, aberrant expression of HDACs is linked to human cancers (Y. Li & Seto, 2016). Class I HDACs, HDAC1, 2, and 3 have been observed to have increased expression in gastric and ovarian cancers (Sudo et al., 2011; Weichert, Denkert, et al., 2008; Weichert, Röske, et al., 2008) and overexpression of HDAC8 is correlated with poor prognosis in neuroblastoma (Oehme et al., 2008; Zhao et al., 2021). Class II HDACs, HDAC6 and HDAC10 are associated with poor prognosis in lung, gastric and hepatocellular cancer (Jin et al., 2014; Lv et al., 2016; Osada et al., 2004). HDAC1, 2, and 3 are highly abundant in lung cancer and are related to poor prognosis (Jung, Noh, Kim, Eun, Bae, Xie, et al., 2012; Minamiya et al., 2010, 2011) while low expression of HDAC5 and 10 are also correlated with poor prognosis in lung cancer (Osada et al., 2004).

Owing to the relationship of HDACs to poor prognosis in cancer and their conserved active sites, this has resulted in robust development of HDAC inhibitors (HDACi) as epigenetic drugs to inhibit the activity of one or multiple HDACs (Witta, 2012). HDACi compounds can generally be grouped into four classes: hydroxamic acid, benzamides, short-chain fatty acids and cyclic peptides. Hydroxamic acid class HDACi are mostly non-selective HDACi that target all Class I, II, and III HDACs. Most HDACi target Class I, II and IV HDACs, which require Zn^{2+} for enzyme activities (Mamdani & Jalal, 2020). The molecular consequences of HDAC inhibition are varied as HDACi have been shown to induce cell cycle arrest, apoptosis, enhance immune responses and inhibit DNA repair, resulting in anti-cancer activities (Miyanaga et al., 2008). The first HDACi used for molecular functional analysis, vorinostat induced expression of p21/CDKN1a in murine erythroleukemia cells leading to cell cycle arrest (Richon et al., 1996) This phenotype was also observed for trichostatin A (TSA), a pan-HDACi, in mouse fibroblast cells (Xiao et al., 1999). HDACi treatment increased c-Jun expression in monocytic leukemia cells (Vrana et al., 1999), reduced Bcl-2/Bcl-xL expression in mesothelioma cells and myeloma cells (X. X. Cao et al., 2001; Fandy & Srivastava, 2006), and attenuated AKT/mTOR signaling leading to autophagy in hepatocellular carcinoma cells (Y.-L. Liu et al., 2010), and suppresses IFN-mediated response by stimulating NF-κB activity, leading to apoptosis in prostate cancer cells (Shulak et al., 2014). HDACi can enhance immune response by up-regulating MHC proteins and inducing costimulatory/adhesion molecules, such as CD40, CD80 and CD86 in myeloid leukemia cells and neuroblastoma cells (Maeda et al., 2000; Magner et al., 2000). HDACi also suppress the expression of DNA repair proteins, including homologous recombination proteins and DNA mismatch repair proteins (Kiweler et al., 2020).

While HDAC inhibitors have shown promising preclinical results for many cancers, clinical trial results vary (Mamdani & Jalal, 2020). Vorinostat monotherapy in non-small cell lung cancer (NSCLC) patients did not show objective antitumor activity, but toxicity with adverse effects such as fatigue (Traynor et al., 2009). Other phase II monotherapy of romidepsin and pivaloyloxymethyl butyrate resulted in little efficacy in patients, and had side effects such as fatigue, nausea, and dysgeusia (Reid et al., 2004; Schrump et al., 2008). One possible explanation is that preclinical studies were all done with selective and non-representative cancer cell lines, which may not be universal to all cancer cases (Begley & Ellis, 2012; Raghavan, 2022). Cellular responses to HDAC inhibition are heterogeneous and depend on factors such as the genetic background, metabolic state, and on-/off-target engagement of individual HDACi

drugs which have the potential to drive non-responsive or adverse responsive effects (Miyanaga et al., 2008). Notably, the majority of available lung cancer cell lines commonly used for lung cancer studies and pre-clinical drug testing have a remarkable imbalance of race and gender, which call for action to establish a database to determine these heterogeneous responses to drugs (Leon et al., 2023).

To determine the mechanisms that drive these heterogeneous cellular responses, we began by quantifying proteome remodeling of HDACi-treated cell lines derived from diverse genetic backgrounds. We chose to explore the effects of hydroxamic acid class non-selective HDACi on proteome remodeling based on cell treatment with belinostat, CUDC-101, trichostatin A (TSA), panobinostat, abexinostat and vorinostat (SAHA). Of these, vorinostat, belinostat and panobinostat have been approved by the FDA for use in T-cell lymphoma and multiple myeloma (Mann et al., 2007; McDermott & Jimeno, 2014; Richardson et al., 2015). We utilized sample multiplexed quantitative proteomic and phosphoproteomic profiling to map proteomic remodeling downstream of epigenetic perturbation in a diverse panel of lung cancer cell lines in response to HDACi treatment (Schweppe et al., 2013; Mitchell et al., 2023). We integrated these data with single-cell transcriptome data to determine how single cell molecular phenotypes drive heterogeneous responses to drug treatments. We found divergent cellular responses to HDACi perturbation were driven by heterogeneous genetic backgrounds. For example, the abundance of some key proteins, like the JUN transcription factor, correlated with the effectiveness of HDACi on cell lines. Additionally, despite binding with their intended HDAC targets, HDACi engaged a large number of off-target proteins, such as AURKB, which may explain adverse effects of HDACi observed in clinical trials. Together these data establish a holistic framework for the molecular characterization of HDACi cellular perturbations with the potential to build on these data by incorporating more diverse cell lines and epigenetic inhibitors.

Result

An automated platform for proteome analysis

To understand how cancer cell lines with diverse genetic backgrounds respond to HDAC inhibition, we screened multiple HDACi by cell line perturbations using an automated high throughput, sample multiplexed proteomics platform. Based on other previous large scale screening work (Mitchell et al., 2023; Nusinow et al., 2020), we designed and applied an automated workflow with an OT2 liquid handler and 96-well-plate-based screening infrastructure (Figure 1A). Six HDACi–belinostat, CUDC-101, trichostatin A (TSA), panobinostat, abexinostat and vorinostat (SAHA)– and one p38 inhibitor outgroup ralimetinib were used to treat 5 cell lines. Strong proteome remodeling was driven by treatment with the six HDACi small-molecules. Of these, belinostat, trichostatin A, panobinostat, CUDC-101 and vorinostat were pan-HDACi while CUDC-101 is an HDACi known to also inhibit HER2 and EGFR activity (Y. Li & Seto, 2016; Shanmugam et al., 2022). Abexinostat mostly targets HDAC1, though it has been shown inhibition to HDAC2, 3, 6, 8, 10. We screened five cancer cell lines, four lung cancer cell lines (A549, H292, PSC1 and PC9, Supplemental table 1) as well as the colorectal cancer cell line HCT116 for comparison to previous chemical proteomic datasets (Mitchell et al., 2023). The four lung cancer cell lines have different genetic and mutational backgrounds derived from adenocarcinomas (A549, PC9, PSC-1) and mucoepidermoid carcinoma (H292). Additionally, the PSC-1 cell line which is derived from

INER-51 cells with P-pg-mediated resistance to small-molecule therapies (Valeria & Raúl, 2005).

As in previous proteomics work to quantify cellular remodeling (Mitchell et al., 2023), cells were incubated with 10 µM of each drug or vehicle control (DMSO) for 24 h prior to viability assays and proteomic analysis. In total, across the 5 separate 16-plex experiments for each cell line we quantified 476,387 unique peptides, 6,615 phosphorylation sites, and 10,621 unique proteins. Protein quantification between biological replicates was reproducible with a median Spearman correlation (r) for biological replicates of each drug and cell line of 0.996 (Supplementary Figure 1A). The median coefficient of variation (%CV) for protein measurements between two biological replicates was 4.4% (Supplementary Figure 1B). Each cell line was quantified to a depth of approximately 8000 proteins (Figure 1C). Among the 10,621 total unique proteins, 5663 proteins were found in all five cell lines, 7922 proteins were found in at least 3 cell lines, and 1633 were found in only one cell line (Figure 1B). In addition to proteomics, we integrated phosphoproteomics, transcriptomics, chromatin remodeling, and thermostability proteomics to elucidate a comprehensive view of lineage-specific remodeling of diverse lung cancer cells in response to targeted epigenetic inhibitors (Figure 1D).

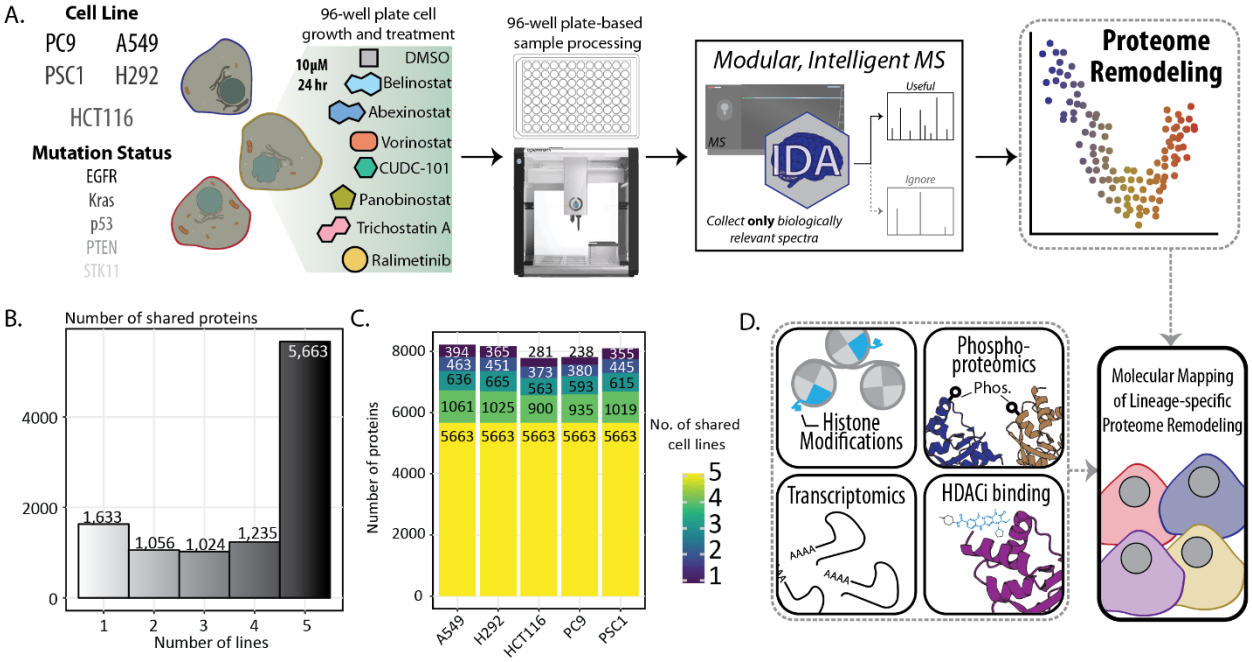

Figure 1 An automated 96-well-plate based lineage-specific proteome remodeling. a, Overview of the workflow, starting with growing five cell lines in 96-well-plates. Sample preparation was performed with OT2 liquid handler after 24 h drug treatment. **b**, coverage of cell lines by proteins. **c**, coverage of proteins by each cell line. **d,** diagram of integration of multi-omics.

Comparison with previous proteome-centric mechanism of action studies

To assess the overall level of HDACi-induced proteome remodeling, we compared our data to previously collected chemical perturbation proteomics datasets. DeepCoverMOA is a proteomic atlas of the drug mechanism of action that tested 875 compounds (Mitchell et al., 2023). Although DeepCoverMOA sheds light on off-target polypharmacology of compounds with comprehensive proteome coverage, HCT116 cells were the only cell line tested. Among the 875 compounds, only vorinostat overlaps with our experiments, so we compared HCT116 treated with vorinostat between our dataset and DeepCoverMOA and found that even though these samples were collected at different times in different labs, they produced highly correlated proteome remodeling ($r_{Pearson}$ = 0.86, slope = 1.01, Figure 2A). More broadly, the proteomic remodeling we observed in HCT116 cells treated with each of the five HDACi compounds resulted in proteomic remodeling that was highly correlated with DeepCoverMOA analysis of HCT116 with vorinostat ($r_{Pearson}$ = 0.74-0.86, Figure 2B) (Mitchell et al., 2023). However, as expected, proteome remodeling with vorinostat treatment in the lung cancer cell lines generate less well correlated molecular responses compared to the DeepCoverMOA analysis of HCT116 cells ($r_{Pearson}$ = 0.34-0.69, Figure 2B).

In HCT116 cells, protein abundance changes resulted from HDAC inhibition were consistent with previous reports: increased abundance of CDKN1A and CCND3 with HDACi (vorinostat, TSA) in T24 bladder carcinoma cells and HT-29 cells (Richon et al., 2000; Siavoshian et al., 2000); increased abundance of c-JUN protein and decreased abundance of HDAC7 with HDACi (TSA) in neuronal cells (Ma & D'Mello, 2011); and reduced abundance of CCNA2 with HDACi (TSA) in H9c2 cells (Majumdar et al., 2012). We observed divergent effects for these proteins across the cohort of cancer cell lines tested. For example, CCNA2 had significantly reduced protein abundance in HCT116 and PC9, but not in the other three cell lines (A549, H292 and PSC1). CCNA2 regulates cell cycle together with CDK1/CDK2, neither of which were observed to have altered protein abundances in any of the treatments presented here (Figure 2C). These data highlight the importance of considerations of the cellular context of cells when assessing mechanism of action and polypharmacology using proteomics.

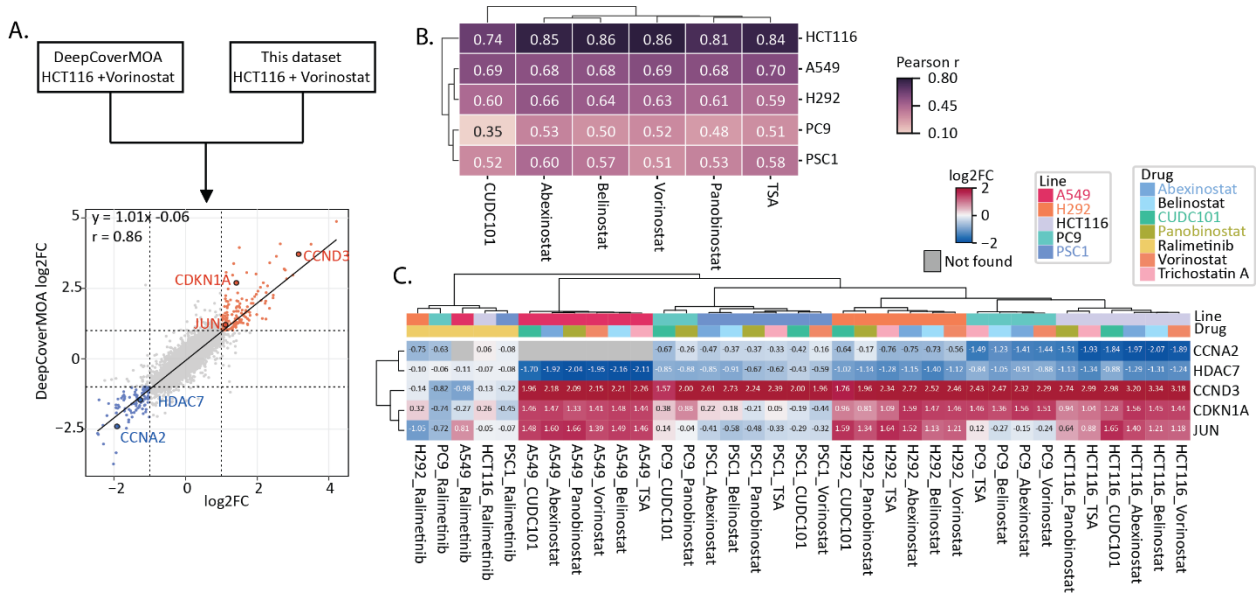

Figure 2 Comparison with DeepCoverMOA data. a, Comparison of HCT116 treated with vorinostat from DeepCoverMOA and our dataset. **b,** Pearson correlation between our 35 CXD groups data and DeepCoverMOA HCT116 treated with vorinostat. **c,** Heatmap of log2FC of proteins mentioned in literature about HDACi treatment.

Cell line viability in response to HDACi or MAPKi

Comparison of our data with DeepCoverMOA revealed considerable cell-type-specific effects of HDACi treatment on the proteomes of perturbed cells (Figure 2A). Based on these findings, we compared the molecular diversity to the effects on HDACi-treated cell viability. As expected, based on the diverse molecular remodeling we observed by proteomics, we found that each of the cell lines had different sensitivity toward the seven tested compounds (Figure 3A). In general, all cell lines except PSC1 had reduced viability when treated with HDACi. PSC1 cells had minimal sensitivity to HDAC inhibition as well as MAPK inhibition (ralimetinib) stemming in part from these cells harboring a P-gp negative mutant derived from INER-51, which has previously been observed to have a P-gp-mediated resistance to chemotherapeutic agents (Valeria & Raúl, 2005). Although PSC1 cells did not express P-gp, these cells have still been observed to be resistant to drugs, such as doxorubicin (Valeria & Raúl, 2005). Conversely, PC9 cells were highly sensitive to HDACi and ralimetinib treatment, especially CUDC-101 (Figure 3A). The increased sensitivity of PC9 cells to CUDC-101 treatment may in part be due to CUDC-101 off-target engagement of EGFR, in addition to HDACs. PC9 cells have a gain of function EGFR mutations driving gene amplifications (Nagai et al., 2005). A549 cells were more sensitive to belinostat treatment compared with other drugs, while H292 and HCT116 cells were consistently sensitive to drug perturbation (Figure 3A).

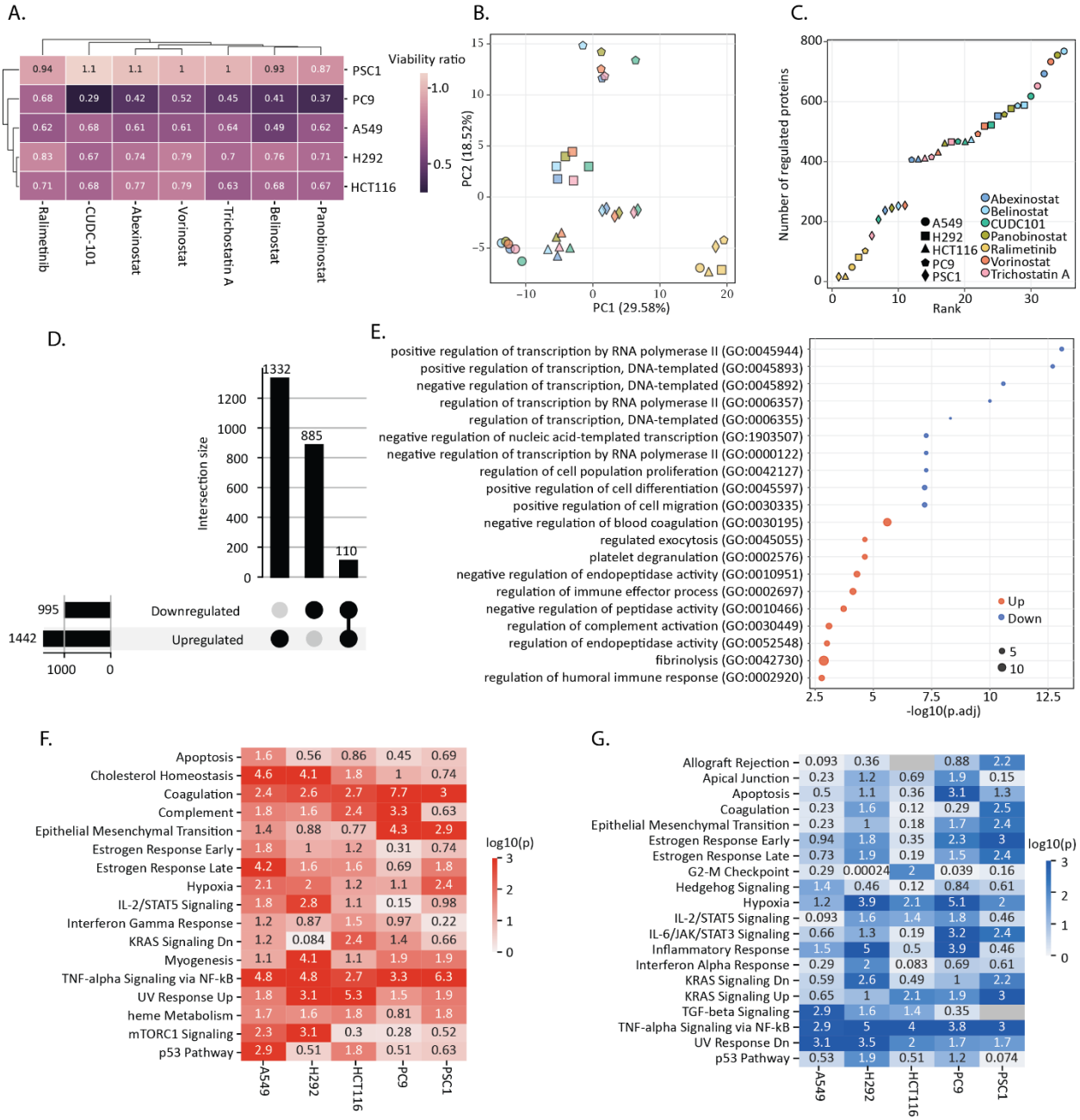

Figure 3 Overall differences between cell lines in response to HDACi or MAPKi. a, viability of each cell line in response to 7 drugs. **b,** Principal component analysis (PCA) of 35 CXD groups. **c,** Waterfall plot highlighting the number of regulated proteins for each CXD group. **d,** Number of regulated events in total. **e,** GO analysis of regulated proteins. **f,** Comparison between cell lines of Hallmark analysis of up-regulated proteins. **g,** Comparison between cell lines of Hallmark analysis of down-regulated proteins.

Quantification of cell line by drug regulatory landscape

Treatment of five cell lines with seven drugs resulted in 35 cell-line-by-drug (CxD) groups. We quantified the relative abundance of proteins in comparison of vehicle (DMSO) controls for each of these perturbations and replicate analyses generated highly correlated proteome abundance shifts (Supplementary Figure 1A). The six HDACi and ralimetinib all have multiple protein targets, which have the potential to drive pleiotropic remodeling of proteins and protein complexes. PCA analysis generally clustered CxD groups based on cell lines, however the ralimetinib-treated cells clustered together in principal component space irrespective of the cell line (Figure 3B).

In total, we observed 14,856 CxD regulated events across all groups on 2,327 different proteins (Supplementary Figure 3A, Supplementary data 1). Among the 2,327 regulated proteins, only 11 proteins were differentially abundant in more than 80% of CxD groups, 85 proteins were regulated in more than 60% of CxD groups and 2,127 proteins were regulated in less than 40% of CxD groups (Supplementary Figure 3A). Based on the total number of regulated proteins A549 cells treated with HDACi had the largest degree of proteome remodeling, followed by H292, PC9, HCT116 and PSC1 cells. While all cell lines treated with ralimetinib had the lowest number of regulated proteins (Figure 3C). The chemoresistant PSC1 cells had the lowest number of regulated proteins among all tested cell lines which is consistent with the limited effect of drug treatment on cellular viability in these cells. Belinostat treatment of lung cancer cells (A549, H292, PC9 and PSC1) consistently generated the largest degree of proteome remodeling, followed by panobinostat, abexinostat, TSA, CUDC-101 and SAHA (Figure 3C). In general, we observed more proteins with increased abundance upon HDACi than proteins with decreased abundance (Supplementary Figure 3B). The one exception was PC9 cells treated with CUDC-101 where more proteins were observed with decreased protein abundance. This may be due to PC9 cells harboring a gain of function EGFR mutation and the off-target engagement of EGFR by CUDC-101 (Nagai et al., 2005; Okabe et al., 2007).

Among the 35 CxD groups, protein abundances tended to have concordant change in only one direction. More specifically, 1,332 proteins were only observed to have increased abundance with drug perturbation while 885 proteins were only observed to have decreased abundance (Figure 3D). Strikingly, only 110 proteins were differentially abundant due to drug treatment across all CxD groups (Figure 3D). Down-regulated proteins mostly were enriched in pathways related to the regulation of transcription (Figure 3E), consistent with perturbation of transcriptional regulation by HDACi treatment. In addition, decreased abundance proteins were enriched for positive regulation of cell differentiation and migration and peptidase and endopeptidase activities. Pathway enrichment analysis of the proteins with increased abundance (Liberzon et al., 2015), revealed pathways consistent with TNF-alpha signaling via NF-kB and UV response pathways (Figure 3F). Notably, some pathways were only significantly regulated in a specific subset of cell lines. For example, mTORC1 associated proteins were only enriched in A549 and H292 cells treated with HDACi. Alternatively, the epithelial-mesenchymal transition pathway was only enriched in PC9 and PSC1 cells. Within the proteins with decreased abundance across CxD groups, all cell lines were enriched for TNF-alpha signaling via NF-kB and UV response down pathways (Figure 3G). Interestingly, proteins involved in p53 pathways mainly had increased abundance in A549 and HCT116 cells, while they had decreased

abundance in H292 and PC9 cells, and these proteins were not differentially regulated in PSC1 cells.

Each cell line has unique regulated proteins, which are quantified in at least three cell lines but only regulated in one cell line (Supplementary Figure 3C). PC9 had the largest number of unique regulated proteins though there was no clear. When assigning cell line -specific and differentially abundant proteins to cancer hallmark enrichment, there was no hallmark pathway significantly enriched in all cell lines (Supplementary Figure 3D, E). For example, proteins in the apoptosis pathway only had increased abundance in HCT116 cells whereas proteins in the mTORC1 signaling pathway had increased abundance on in A549 cells and proteins associated with the interferon alpha response had increased abundance in A549 cells but decreased abundance in H292 and PSC1 cells.

Isoform specific perturbation of HDAC abundance

The abundance of HDAC proteins after HDACi treatment across CxD groups was highly variable (Figure 4A). We quantified 10 of the 11 human HDAC proteins in our samples as well as additional isoforms of HDAC7 and isoforms of HDAC9. Although there is no evidence that HDAC7 and HDAC9 are related with lung cancer progression, HDAC7 and HDAC9 are associated with poor prognosis of other cancers, such as pancreatic cancer and medulloblastoma (Y. Li & Seto, 2016). For HDAC7 we observed, HDAC7 isoform 5 (HDAC7-5, 96% sequence similarity), and HDAC7 isoform 8 (HDAC7-8, 88% sequence similarity). Neither of these HDAC7 isoforms have established cancer-related functions compared to the canonical HDAC7. Compared with the canonical HDAC9 sequence, HDAC9 isoform 7 (HDAC9-7) has 94% similarity which affects the cellular localization, and HDAC9 isoform 10 (HDAC9-10) only has 57% similarity. HDAC9-10 is truncated and missing its histone deacetylase domain. Most HDACs were not significantly regulated, only HDAC7-8 and HDAC9 were significantly regulated. HDAC7-8 was only found and down-regulated in A549, H292 and HCT116, while HDAC7-5 was only found in PC9 and PSC1 cells and not significantly regulated. HDAC7 was shown to have reduced expression when treated with TSA in neurons (Ma & D'Mello, 2011). HDAC9-7 was found in A549, H292, HCT116 and PSC1 and it was up-regulated in A549, but down-regulated in PSC1. HDAC9-10 was found only in PC9 cells and it was down-regulated.

Although HDAC7 and HDAC9 were regulated in some cell lines, known interacting proteins for these proteins did not have significant differences in protein abundance. However, abundance fold change after treatments of two HDAC7 interacting proteins, ADNP and FLYWCH2, had a strong correlation with HDAC7 (Figure 4B). ADNP was positively related to HDAC7 with a correlation coefficient of 0.88 (Figure 4C). ADNP is a zinc finger protein, involved in transcriptional activity (Zamostiano et al., 2001). It plays roles in tumorigenesis related to cancer growth and proliferation. However, the function of it is not clear. On one hand, ADNP was reported up-regulated in colon cancer cells and bladder cancer cells (Blaj et al., 2017; Zhu et al., 2020). On the other hand, silencing of ADNP led to an increase in cell proliferation in colon cancer and breast cancer cells (Blaj et al., 2017; Rangel et al., 2017). ADNP can activate MAPK/ERK and PI-3K/Akt pathways in neuronal cells (Pascual & Guerri, 2007). Inhibition of ADNP can increase p53 expression (Zamostiano et al., 2001). FLYWCH2, a zinc finger protein, had moderately increased abundance with HDACi treatment in the tested cell lines, and FLYWCH2 abundance was negatively correlated with HDAC7 with a correlation coefficient of 0.63 (Figure 4D). While the exact function of FLYWCH2 in cancer progression is not well

explored, it has significant prognostic performance in pancreatic and cervical cancers (Uhlen et al., 2017). These HDAC specific responses across CxD treatment groups highlight the potential to uncover new potential mediators of chromatin regulation in cancer cells.

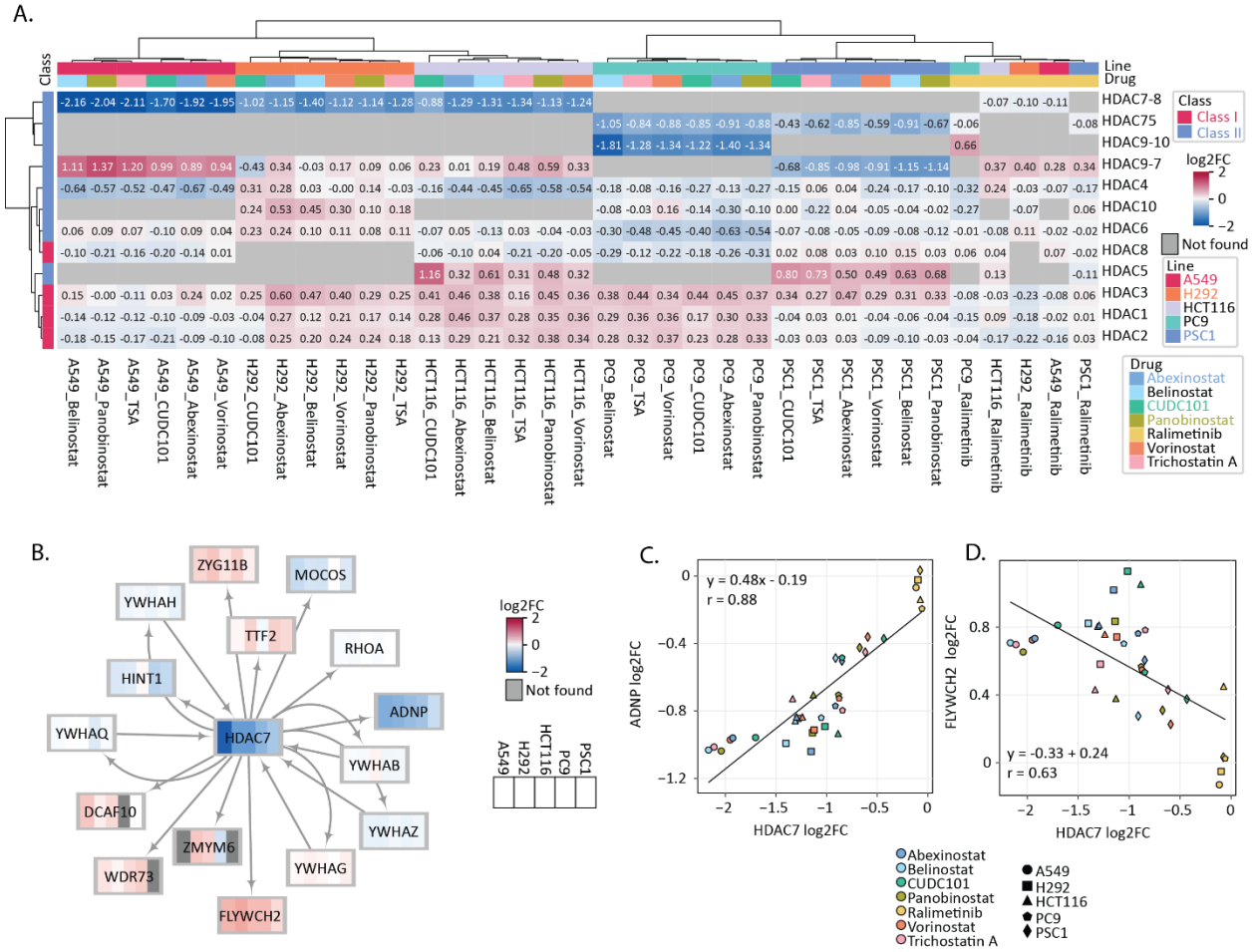

Figure 4 Difference between cell lines of HDACs. a, Heatmap of log2FC of HDACs in 35 CXD groups. **b,** HDAC7 protein network. Means of protein regulation of each cell line were shown. **c,** Correlation between HDAC7 and ADNP protein log2FC. **d,** Correlation between HDAC7 and FLYWCH2 protein log2FC.

Regulation of constituent of the HDAC pathway

Most proteins involved in the HDAC pathway (n=76 proteins) were not regulated after HDACi treatment (Supplementary Figure 5A). Yet, among them we quantified 21 proteins–27% of the HDAC pathway–that were significantly regulated in at least one cell line after HDACi treatment. Among them, the Jun transcription factor (c-Jun) had a significant increase in protein abundance in A549, H292, and HCT116, but not PC9 and PSC1 (Figure 5A). The Jun transcription factor has multifaceted outputs of biological activities. Activation of c-Jun induces cell proliferation and differentiation, though it has a contradictory effect on apoptosis depending on the cell type(Papavassiliou & Musti, 2020). HDAC1 and c-Jun form a protein complex in the c-Jun N-terminal kinase (JNK) pathway which is an important pathway involved in apoptosis and inflammation (Sanna & Galeotti, 2018). HDAC6 activates c-Jun and JNK pathway, but functions as tumor suppressor in liver cancer or tumor promoter in gastric cancer (Jung, Noh, Kim, Eun, Bae, Chang, et al., 2012; Huang et al., 2020). While both HDAC1 and HDAC6 activate c-Jun and JNK pathway, HDAC7 and HDAC9 inhibit c-Jun expression and JNK pathway (Morrison et al., 2006; Ma & D'Mello, 2011). c-Jun protein abundance was significantly increased in A549, H292 and HCT116, where HDAC7 was significantly down-regulated in the three cell lines. Interestingly, this result was consistent with previous reports of HDACi (TSA) treatment in neuronal cells (Ma & D'Mello, 2011). However, in PC9 and PSC1, neither c-Jun nor HDAC7 protein abundances were significantly regulated. Interacting proteins of c-Jun also showed differences in protein abundance across cell lines. JunB, a transcription factor from the same family as c-Jun, was significantly down regulated in H292 and PC9, but slightly upregulated in A549, HCT116 and PSC1. The same trend was also observed in c-FOS, a protein that forms heterodimer with c-Jun and JunB and plays an important role in cell development. The c-FOS was significantly upregulated in A549, HCT116 and PSC1, but was not found in H292 and PC9.

We tested the correlation between the 10 HDACs we quantified and the 5,491 other proteins that were quantified in all samples (Supplementary table 2). Of these, we observed 87 proteins had correlated abundance profiles with at least one of the HDAC proteins ($r_{Pearson} > 0.9$, Supplementary figure 5B). Though we did not observe significant enrichment of specific biological processes within these data, we did observe strong correlation with HDAC7 among the 87 proteins. In fact, 76% of these proteins (66 of 87) were observed to be correlated with HDAC7 protein abundance (Supplementary Figure 5C). In addition, 15 correlated with HDAC9 (Supplementary Figure 5D). These proteins showed cell line specific changes which are similar to HDAC7 and HDAC9 changes. Notably, in addition, HDAC1 and HDAC2 protein abundance was well correlated across datasets and had a correlation coefficient of ($r_{Pearson} = 0.92$). Of these proteins, the most highly correlated proteins were 3 of them having a correlation coefficient larger than 0.95, namely SRC, MICALL1 and FUCA1 (Figure 5B, C, D). SRC is a proto-oncogene tyrosine-protein kinase, involved in events such as cellular transformation, tumorigenesis and metastasis. SRC is activated in non-small cell lung cancers (J. Zhang et al., 2007), but HDACi can reduce SRC expression in colon cancer cells (Hirsch et al., 2006) which is consistent with our observation in lung cancer cells. HDAC3 phosphorylation by SRC has also previously been suggested as a key process for breast cancer cells proliferation and invasion (Longworth & Laimins, 2006; Matteucci et al., 2007; Kwak et al., 2019). While HDAC3 phosphorylation was not observed in our samples, there was also no significant correlation between HDAC3 and SRC protein abundance ($r_{Pearson} = 0.11$). Thus, these data suggest a relationship between SCR and HDAC7 in response to HDACi or epigenetic perturbation in lung

cancer cells. While there was limited functional information about the role of MICALL1 (Molecule Interacting with CasL-like 1) in cancer, we found previous evidence that MICALL1 may act downstream of p53 in the regulation of tubular recycling endosome biogenesis (Takahashi et al., 2017), or as a downstream effector of EGFR signaling in the regulation of malignant growth and invasion of metastatic cancers (Dymova et al., 2022). Furthermore, from our data, MICALL1 protein abundance in response to HDACi treatment was highly correlated with HDAC7 ($r_{Pearson} = 0.96$) and SRC ($r_{Pearson} = 0.90$). FUCA1 is a fucosidase. The p53 up-regulates FUCA1 expression by inducing its transcription (Tsuchida et al., 2017). FUCA1 expression has been observed to increase after some drug treatments, such as doxycycline (Baudot et al., 2016). These observations were consistent with our HDACi treatment data that FUCA1 expression increased after HDACi treatments. In addition to these three proteins (SRC, MICALL1, FUCA1), we observed cancer-related proteins with high correlation ($r_{Pearson} > 0.9$) with HDAC7, such as the receptor tyrosine kinase signaling adapter protein GRB2 (Lowenstein et al., 1992; Ding et al., 2019; Yang et al., 2021) and the p38 kinase activator MAP2K3 (Raingeaud et al., 1996) (Figure 5E, F).

Among the 15 proteins correlated with HDAC9 (Supplementary Figure 5C), the top two were the sodium-dependent vitamin C transporter SLC23A2 and the Myc target gene RIOX2 (Figure 5G, H). Both SLC23A2 and RIOX2 have previously been associated with poor prognosis in cancer (Teye et al., 2004; Komiya et al., 2010; Duell et al., 2013). Interestingly, the histone demethylase RIOX2 has been previously associated with cell growth and cancer cell development (Q. Zhang et al., 2020; Y. Zhang et al., 2005) and overexpression of RIOX2 was previously found to induce EGFR expression (Komiya et al., 2010). PC9 cells harbor an EGFR mutant (E746−A750del) and were the only cells we observed with significantly lower protein abundance for HDAC9 while the protein abundance of RIOX2 did not change after HDACi treatment. These data suggest that both RIOX2 and HDAC9 activities may be directly affected by the EGFR signaling state of the treated cells. The specific molecular linkage of HDAC7 and HDAC9 abundance to key drivers of oncogenesis and cancer progression suggests routes for targeted, and potentially isoform specific therapies for these two HDACs may overcome previous challenges with HDAC inhibition in lung cancer cells.

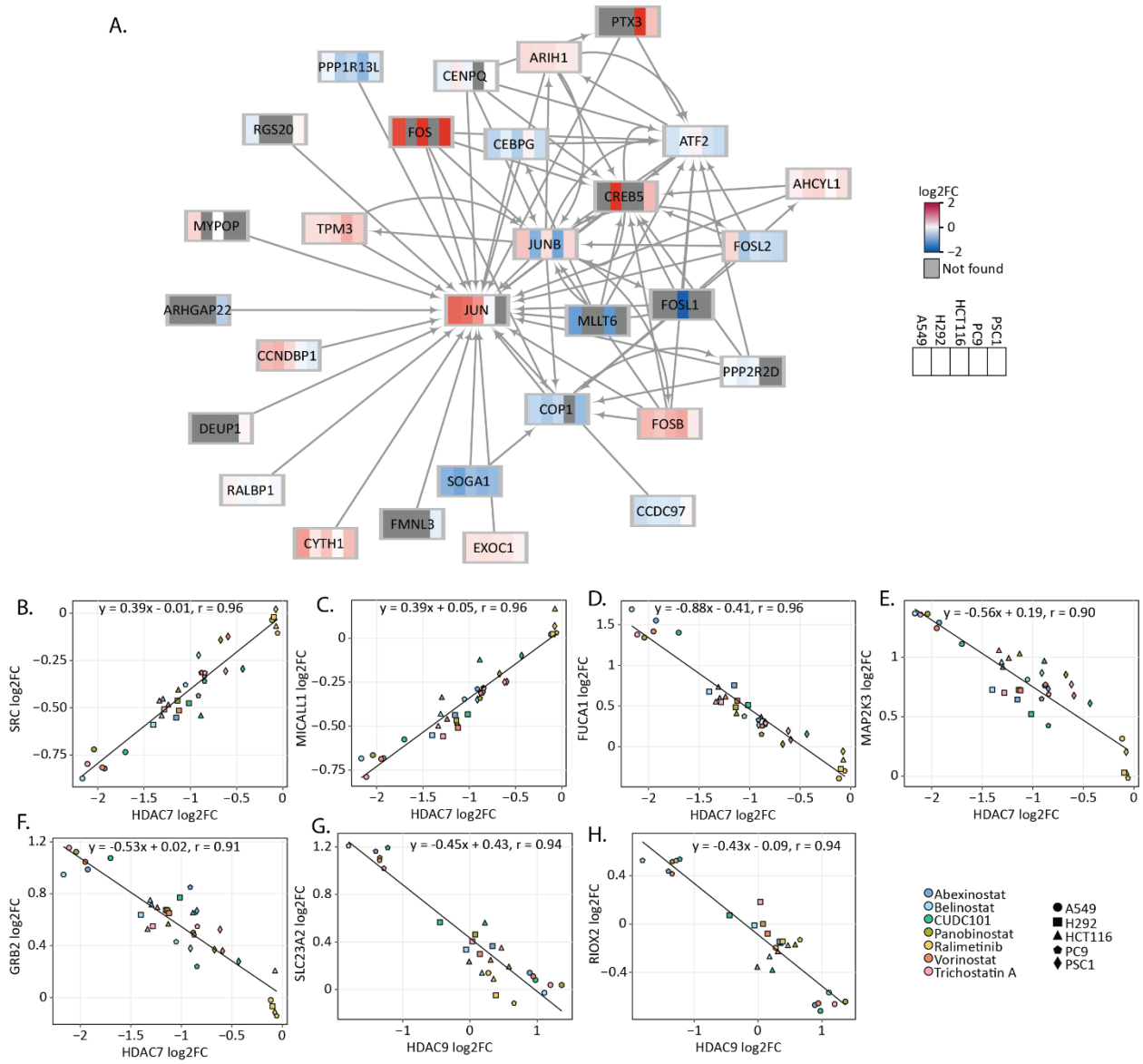

Figure 5 Difference between cell lines of proteins from the HDAC pathway. a, JUN protein network. Means of protein log2FC of each cell line were shown. **b, c, d, e, f,** Correlation between HDAC7 with SRC, MICALL1, FUCA1, MAP2K3 and GRB2. **g, h,** Correlation between HDAC with SLC23A2 and RIOX2.

Post-translational response to HDAC inhibition

Owing to the widespread remodeling of CxD group proteomes, we sought to determine if post-translational modifications could similarly be used to differentiate key effectors of HDACi responses in diverse cell lines. To this end, we performed quantitative phosphoproteomics to quantify a total of 8787 phosphorylation sites, including 1363 regulated phosphosites (Supplementary data 2). Among the 35 CxD groups, 457 phosphosites were only observed to have increased abundance upon HDACi treatment, 526 sites were only observed to have decreased abundance upon treatment, and 190 sites were observed to have both increased and decreased abundance across CxD groups. We ranked each CxD group based on the number of regulated phosphosites. PC9 cells treated with HDACi had the largest number of regulated sites, followed by H292, A549, HCT116 and PSC1 cells. Interestingly, all cell lines treated with ralimetinib had the fewest regulated phosphosites (Figure 6A). Overall, most groups had more sites with increased abundance than sites with decreased abundance. The exceptions were PC9 cells which had significantly more down regulated sites than up regulated sites when treated with TSA, panobinostat and CUDC-101 (Figure 6B). When compared with regulated proteomics data, we generally observed concordance between the number of regulated proteins per CxD group and the number of regulated phosphosites. (Figure 6C).

We explored HDACi regulated events based on phosphosites which were regulated with no corresponding change in protein abundance (phospho-specific regulation). In total, we observed 1622 phospho-specific effects for 975 proteins (Supplementary Figure 6A). These sites showed limited consistency across CxD groups with no phospho-specific regulation found in all 35 CxD groups, though we did observe that each group had multiple phospho-specific effects (Figure 6D). For example, in PC9 cells we observed the largest number of phosphosites-specific regulation. Protein AHNAK had the most phosphospecific regulations in 22 CxD groups. AHNAK is a scaffold protein, involved in cell signaling and tumor metastasis (Davis et al., 2014). It has increased phosphorylation level in cancer cells with FGRF inhibitor treatment (PD173074) (Pal et al., 2006). In H292 and PC9 cells, AHNAK phosphosites were mostly downregulated, but in PSC1, AHNAK phosphosites were upregulated (Supplementary Figure 6B). Yet, the phospho-specific regulated proteins were involved in similar pathways among 5 cell lines. Consistent with the cell-cycle effects of HDAC inhibition, we observed phospho-specific regulation enriched for the G2-M checkpoint, mitotic spindle and Myc targets V1 pathways in all 5 cell lines (Supplementary Figure 6C, D).

We tested the correlation between HDAC7/9 and 681 phosphosites that were quantified in at least 28 CxD groups (Figure 6E). Of these, 10 phosphosites were observed to be correlated with HDAC7 protein abundance ($r_{Pearson} > 0.8$, Figure 6F) and two phosphosites were correlated with HDAC9 protein abundance ($r_{Pearson} > 0.8$, Figure 6G). Among them, BAD Ser118 was correlated with HDAC7 ($r_{Pearson} = 0.85$), while BAD protein abundance was not correlated ($r_{Pearson} = 0.13$). BAD is an apoptotic protein that promotes cell death by forming a protein complex with anti-apoptotic proteins Bcl-2 and Bcl-xL (Gajewski & Thompson, 1996). Phosphorylation on BAD Ser118 by PAKs (p21-activated kinases) leads to dissociation of BAD from the complex, which then suppresses cell death (Daniels & Bokoch, 1999). BAD protein had reduced protein abundance only in PC9 with HDACi treatment, while BAD Ser118 had increased abundance in A549, H292 and HCT116, but not PC9 and PSC1 (Figure 6G). However, PAKs protein abundances were not regulated in our dataset, potentiating the idea that redundant kinase activity

may drive phosphorylation of BAD Ser118 in response to HDACi. To find the potential kinase that phosphorylated BAD Ser118, we tested the correlation between BAD Ser118 and 248 kinases that were quantified in at least 28 samples. Of these, we observed 7 kinases correlated abundance profiles with BAD Ser118 ($r_{Pearson} > 0.8$, Figure 6H). These included MARK4, NRBP2, AKT1, SRPK2, PDK2, RPS6KC1, ADCK5, and MKNK1. BAD Ser118 has a 'RR-x-S' motif, and none of these proteins belong to the canonically associated family of cAMP- and cGMP-dependent protein kinases (Glass et al., 1986; Glass & Smith, 1983). Yet, motif analysis using KinasePredictor (Poll et al., 2024) suggest that AKT1 ($score_{KinasePredictor}$=1.84), SRPK2 ($score_{KinasePredictor}$=1.59), and MARK4 ($score_{KinasePredictor}$=0.58) may be able to recognize 'RR-x-S' motif based on their canonical recognition motifs: AKT1 ([RN]-x-[RK]-T-A-[ST]-[FYV]-[IS]-D-K-V), SRPK2 (R-x-x-[STY]-P-x-P) and MARK4 (K-[RK]-[WS]-G-[SY]-V-E-[DN]-[LI]) (Poll et al., 2024; Sugiyama et al., 2019).

These data highlight that HDACi treatment altered not only protein regulated pathways, but also phosphorylation-regulated pathways. Interestingly, each of these signaling pathways were affected irrespective of the genetic background of the cell lines. Together, the combination of proteomics and phosphoproteomics integrated understanding of overall proteome remodeling and the consistent dynamics of cell signaling networks downstream of HDACi treatment.

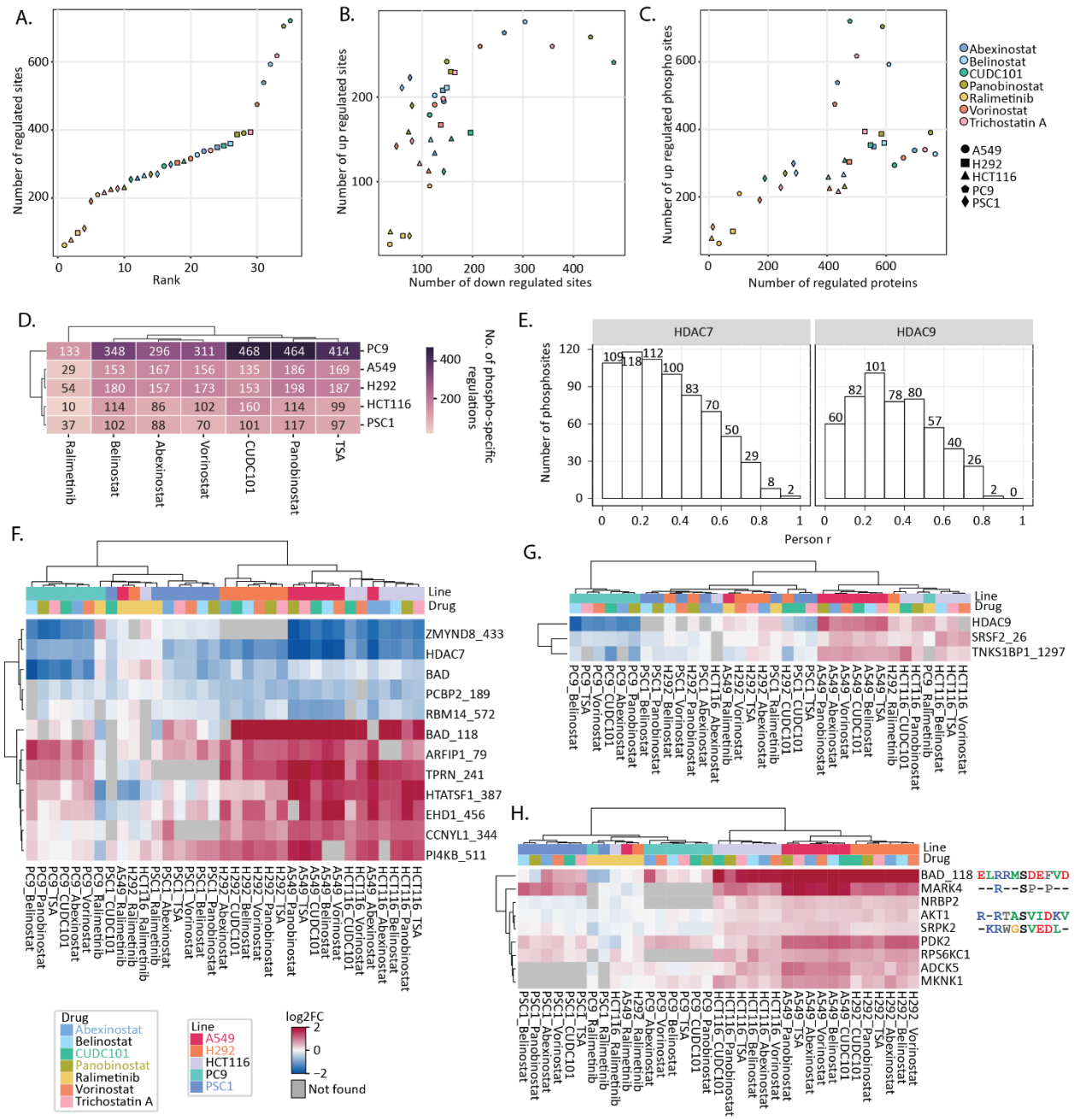

Figure 6 Difference between cell lines of phosphorylation with HDACi treatments. a, Waterfall plot highlighting the number of regulated phosphosites for each CXD group. **b,** Activity of each CXD group measured by the number of phosphosites down-regulated (x axis) and up-regulated (y axis) after 24 h treatment. **c,** Activity of each CXD group measured by the number of regulated proteins (x axis) and regulated phosphosites (y axis) after 24 h treatment. **d,** Heatmap of number of phospho-specific regulations in 35 CXD groups. **e,** Number of phosphosites correlated with HDAC7 and HDAC9 abundance. **f,** Heatmap of phosphosites correlated with HDAC7. **g,** Heatmap of phosphosites correlated with HDAC9. **h,** Heatmap of proteins correlated with BAD ser118.

Coordinated remodeling of the transcriptomes and proteomes of chemically perturbed cells

We next sought to understand the level of concordance between the transcriptome and proteome effects downstream of epigenetic perturbation of lung cancer cells. We compared our A549 perturbed proteomics data of established transcriptome data for matched cell and treatment conditions (Srivatsan et al., 2020). Cell responses generated distinct clusters based on treatments on both single cell level and bulk level (Figure 7A). In response to HDACi treatments, A549 cellular proteomes and transcriptomes were correlated ($r_{Pearson}$ = 0.48-0.64) (Figure 7B), consistent with previous proteomics and transcriptomics comparisons ($r_{Pearson}$ = 0.42-0.57) (Wang et al., 2019). For example, panobinostat treatment resulted in consistent molecular responses for both the proteome and the transcriptome in A549 cells ($r_{Pearson}$ = 0.64).

Transcript data were pulled from recent single-cell chemical transcriptomics work. Even though a single lung cancer cell line was used, we observed diverse single cell responses to HDACi perturbation (Figure 7A). We pseudo-bulked these single-cell data for comparison to our bulk proteomics analyses and grouped proteins/transcripts into nine groups based on significant changes in proteomic and transcriptomic responses in A549 cells treated with abexinostat, belinostat, panobinostat, or TSA (Figure 7B, Supplementary Figure 7A). For example, proteins in Group 1 had high RNA expression but low protein abundance after HDACi treatment and Group 3 had concordant high RNA expression and high protein abundance (Supplementary Figure 7A).

Group 3 and group 7 were proteins that had concordant significant changes in both proteomics and transcriptomics and represented a total of 505 proteins. The proteins in these groups were enriched for oncogenes and tumor suppressors, with notable effects of increased abundance of JUN, FOS, CDKN1A and MAP2K3, and reduced abundance of HDAC7, ADNP, BCL3 and CCND1 (Figure 7B). Enrichment analysis further highlighted that these proteins were involved in mTORC1 signaling, cholesterol homeostasis, coagulation, estrogen response late, myogenesis, TNF-alpha signaling via NF-kB and the p53 pathway (Supplementary Figure 7B, C). Notably, these were pathways we observed consistently responding to HDACi treatment in A549 cells (Figure 3F, G). Group 2 and group 8 contained proteins that had significant changes measured by transcriptomics but not by proteomics and represented the majority of protein measurements observed with 4,805 proteins (87% of proteins quantified across all cell lines). Group 2 proteins also mostly overlapped with A549 regulated pathways when treated with HDACi, but group 8 proteins were largely involved in some unique pathways, such as E2F targets, G2-M checkpoint and Myc targets V1, V2 pathways (Supplementary Figure 7D, E).

We investigated the proteins in the discordant regions of the transcriptomic and proteomics response (Groups 1, 4, 6, and 9, Figure 7B). As mentioned earlier, CCND3 (cyclin D3) abundance consistently increased across cell lines after HDACi treatments (Figure 2C), but CCND3 transcripts decreased in A549 with HDACi treatments (Figure 7B). These changes were observed in a previous study about TSA (Siavoshian et al., 2000). D type cyclins (D1, D2, D3) bind CDK4/6 and sequester CDK inhibitor proteins CDKN1A/p27 and facilitate CDK2/cyclin E and CDK4/6 activities to enable progression through the cell cycle (Sawai et al., 2012). CDKN1A inhibits CDK4 kinase activity, but also assists assembly of cyclin D-CDK4 complexes (LaBaer et al., 1997; Bockstaele et al., 2006). We observed that CDK4 did not have significant transcript or protein abundance change, while CDK6 had reduced protein abundance in A549 and H292 and CDKN1A had increased protein abundance in all cell lines except for PSC1

(Figure 7C). As CCND3 can form a complex with CDKN1A, these data may suggest that CCND3 is stabilized in the nucleus with CDKN1A upon HDACi treatment, but not other components of the complex, such as CDK4 and CDK6.

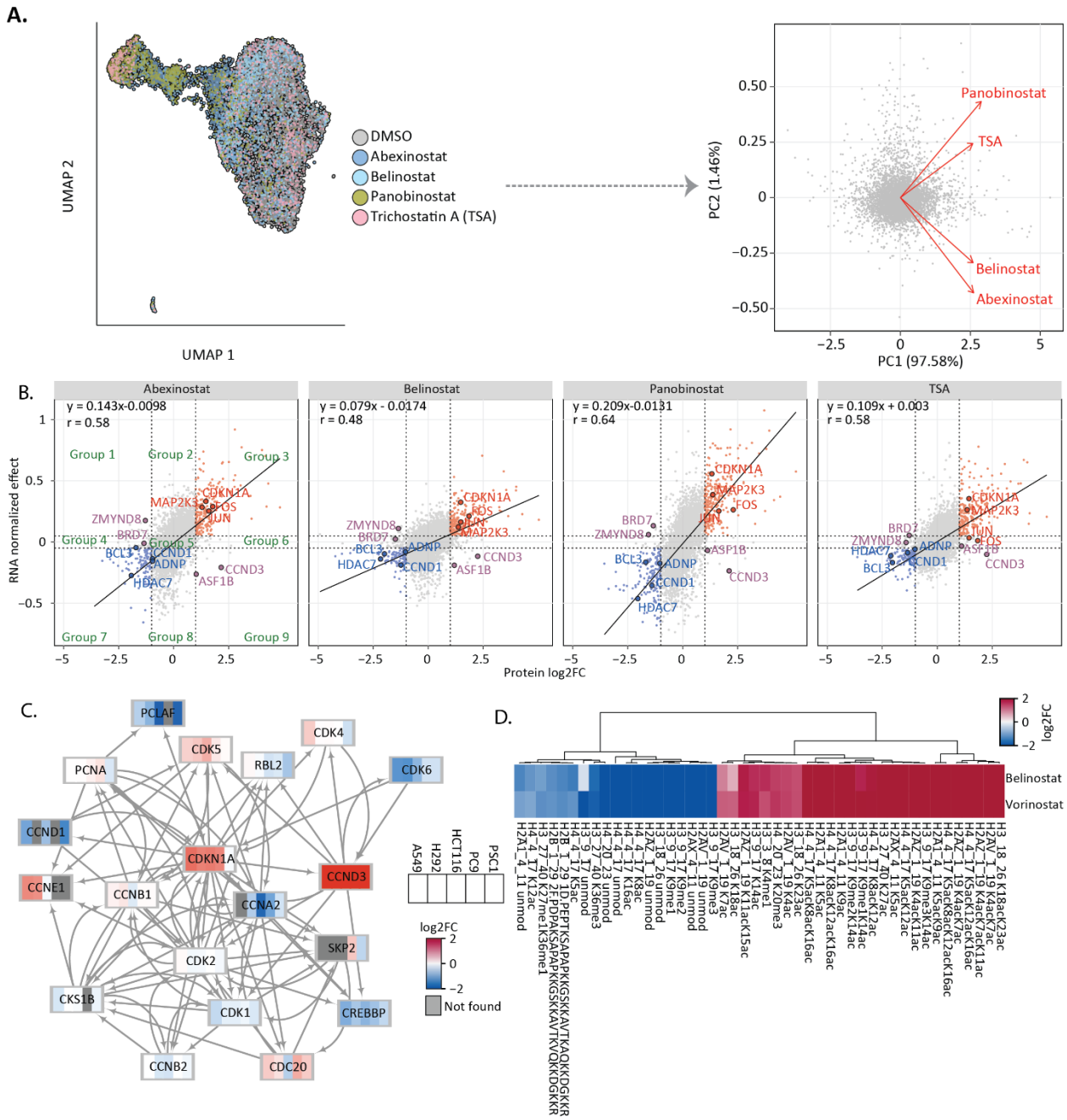

Figure 7 Coordination between transcriptomes, proteomics and histone modification in A549 with HDACi treatments. a, UMAP analysis of single-cell transcriptomics and PCA biplot of bulk transcriptomics. **b,** Activity of A549 treated with 4 HDACi by the protein log2FC (x-axis) and RNA normalized effect (y-axis). The regulated proteins were defined as absolute log2FC versus DMSO larger than 1 in proteomics dataset and absolute normalized effect larger than 0.05 in transcriptome dataset. Based on the four thresholds, proteins were grouped into 9 clusters. **c,** Protein network of CDKN1A and CCND3. **d,** Heatmap of regulated histone modification in A549 with HDACi treatments.

Coordinated remodeling of histone modification and proteomes of chemically perturbed cells

In addition to CCND3 mentioned above, ASF1B, ZMYND8 and BRD7 stood out owing to their discordant transcript and protein abundances (Figure 7B) and their known roles in interacting with histones and histone specific modifications, especially H3K14ac. To gain further insight into the molecular effects of HDACi treatment (vorinostat and belinostat), we investigated how these drugs remodeled chromatin based on the changes in histone modifications status. After HDACi treatment, 19 distinct histone modifications had decreased abundance, most of which were histone methylations, while 27 modifications had increased abundance. As expected, those with increased abundance were predominantly acetylation events (Figure 7D). For example, H3K27ac increased and H3K36me3 decreased after HDACi treatment as expected (Govers et al., 2019; Tharkar-Promod et al., 2018). Thus, these data offer molecular clues that link HDACi protein inhibition and transcriptomic and proteomics remodeling.

ASF1B is a histone chaperone that recognizes H3K9me1 and imports H3 from the cytosol to the nucleus, where it forms a complex with H3K14K18ac (Alvarez et al., 2011). The histone modification data showed that H3K9me1 was downregulated while H3K14ac and H3K18ac were both up-regulated with HDACi treatment (Figure 7D), which was consistent with the increased abundance of ASF1B. These data suggest a model whereby upon HDAC inhibition by an HDACi, increased levels of H3K14K18ac sequester ASF1B and prevent ASF1B release and transit out of the nucleus. Thus, although the transcript abundance of ASF1B did not change significantly, if ASF1B protein was trapped in the nucleus it may be protected from degradation. As ASF1B overexpression promotes proliferation of cancer cells (X. Liu et al., 2020), this may represent a route by which cells bypass HDAC inhibition.

We observed that both the zinc-finger protein ZMYND8 and the bromodomain protein BRD7 had consistent decreases in protein abundance with HDACi treatment (Figure 6). ZMYND8 recognizes dual histone mark H3K4me1/H3K14ac or H3K36me2/H4K16ac to suppress tumor-related genes (Adhikary et al., 2016; N. Li et al., 2016; Mukherjee et al., 2020). H3K4me1/H3K14ac were both up-regulated, while H3K36me2/H4K16ac were both down-regulated with HDACi treatment (Figure 7D). BRD7 also binds to H3K14ac (Cong et al., 2006, p. 200). BRD7 is mainly found in the nucleus and nuclear localization of BRD7 suppresses tumor proliferation (M. Zhou et al., 2006). We noted that protein abundance of both ZMYND3 and BRD7 engaging H3K14ac consistently reduced, which was inverted from the phenotype we observed for ASF1B, also engaging H3K14ac (Supplementary Figure 7F). These data may suggest that ASF1B occupancy of H3K14ac sites excludes ZMYND3 and BRD7 which in turn would free these proteins to be degraded in a PARP-1 or anaphase-promoting complex dependent manner (Hu et al., 2019).

In summary, although regulated events were involved in the same signaling pathways, neither the proteomics nor transcriptomics data comprehensively represented the biochemical changes in these cells. Only by integrating proteomics, transcriptomics and histone modification data were we able to suggest models of epigenetic regulation downstream of HDACi treatment and generate new testable hypotheses about histone binding and sequestration.

Protein-drug engagement indicates potential mechanistic routes for divergent cellular responses

Having established the divergent molecular phenotypes in response to HDACi treatment across cell lines, we next sought to determine what the direct drivers of these differential effects might be. To do this we performed thermal stability analysis (Gaetani et al., 2019; Van Vranken et al., 2021) of HDACi treated A549 cells (Gaetani et al., 2019; Van Vranken et al., 2021) (Figure 8A). While the whole cell proteomics profiling provides information about the stable state of cells after drug treatment, thermal stability analysis can specifically identify HDACi-protein engagement. For example, we compared total proteomics and thermal stability analyses after belinostat treatment to integrate understanding of early HDACi action (thermal stability) and downstream effects (total proteomics) (Supplementary Figure 8A, B, D). Owing to the potential importance of cellular and chromatin context in affecting HDACi engagement, we have previously found that both cell- and lysate-based analyses were complementary for deciphering the molecular effects of chemical perturbations in cancer cells (Van Vranken et al., 2024). From the thermal stability analysis, we observed clear engagement of belinostat and vorinostat with HDAC1, HDAC2, HDAC6 (Figure 8B). We know from quantification of histone modifications in matched A549 cell treatments that histone acetylation increased as expected on H3K27ac, while histone methylation on these residues decreased due to HDACi treatment (Figure 7B). Thus, for example, we can recapitulate the canonical mechanism of action whereby HDACi engaged with HDAC1/2 promoting histone acetylation. Strikingly, we also observed a large number of off-target proteins with large thermal stability changes in both cells and lysates including engagement of defender against cell death 1 (DAD1), fatty acid desaturase 1 (FADS1) and spindle associated kinases (AURKB) (Figure 8C).

From our thermal stability analysis, we observed consistent engagement of HDACi with both HDAC1 and HDAC2. Yet, belinostat treatment did not significantly affect the protein abundance for either HDAC1 or HDAC2 (Figure 8B). Although HDAC1/2 abundances were unaltered, we did observe significant changes in protein abundance for other components of the polycomb repressive complex PRC1 and interacting proteins (Figure 8D). For example, HDACi treatment thermally destabilizes the transcription factor MGA and the EHMT1/2 histone methyltransferase (Figure 7C). Both proteins are known to act downstream of HDAC1/2 and PRC1 (Chittock et al., 2017) as repressors of E2F- and Myc-responsive genes (Ogawa et al., 2002), and HDACi and EHMT1/2 inhibitors can synergistically improve antineoplastic activity compared to using HDACi alone (Bamberg et al., 2022). Interestingly, we observed no significant effect on the abundance of either MGA or EHMT1 in living cells after belinostat treatment (Figure 8D). We also observed thermal destabilization of the zinc finger protein ZMYM3, which is part of the BHC histone deacetylase complex that also includes HDAC1/2 and facilitates DNA repair at damaged chromatin (Hakimi et al., 2003; Leung et al., 2017). Destabilization of downstream interacting proteins of HDAC1/2 suggests that these proteins may engage belinostat or that HDACi treatment drives remodeling of the BHC deacetylase complex upon HDAC1/2

engagement of belinostat (Van Vranken et al., 2024). Additionally, we observed two transcriptional factors upstream of HDAC1/2, TGIF2LX and TRPS1, that did not engage with HDACi based on thermal stability data, but their protein abundance increased significantly with HDACi treatment (Figure 8D). TGIF2LX belongs to a family of proteins that act as transcriptional repressors of transforming growth factor β (TGFβ) that can recruit HDAC1 (Melhuish et al., 2001). TRPS1 recruits HDAC2 in the control of cell cycle and proliferation (Wu et al., 2014). These data suggest that cells may try to compensate for HDACi treatment by increasing expression and abundance of two specific regulators of HDAC activity providing molecular clues for potentially synergistic avenues of therapeutics in lung cancer cells.

Finally, our thermal stability data identified putative off-target protein engagement of belinostat (Figure 8C). DAD1 and FADS1 were significantly stabilized by belinostat in the thermal stability assay. DAD1 is an anti-apoptotic protein (Sugimoto et al., 1995) and a component of oligosaccharyltransferase (OST) complex (Roboti & High, 2012) as well as a prognostic marker in liver cancer (Uhlen et al., 2017). FADS1 is a prognostic marker in renal cancer, urothelial cancer and thyroid cancer (Uhlen et al., 2017). Interestingly, we also observed that SIRT2 (NAD-dependent protein deacetylase sirtuin-2) which acts upstream of FADS1 and can inhibit NSCLC cell growth (Z. Li et al., 2016) had increased protein abundance upon HDACi treatment and was thermally destabilized in our cell thermal stability assay (Supplementary Figure 8C). In addition to DAD1 and FADS1, AURKB was destabilized by belinostat in thermal stability (Figure 8C). Overexpression of AURKB can inhibit p53 transcriptional activity and leads to poor prognosis in NSCLC (Smith et al., 2005; Al-Khafaji et al., 2017) and while AURKB abundance did not increase after HDACi treatment, we did observe that the AURKB interacting protein TUBB2A, a cancer-promoting protein (Shin et al., 2020), had increased protein abundance in our data (Figure 8E). Thus, our data offer insights into routes by which HDACi compounds engage off-targets such as DAD1, FADS1, and AURKB that may synergize with the goal of inhibiting cancer proliferation. Together, the integration of HDACi engagement data enables dissection of potential mechanisms of lineage specific effects in response to HDACi, and provides complementary data to the combined total proteomic, transcriptomic, and chromatin remodeling data.

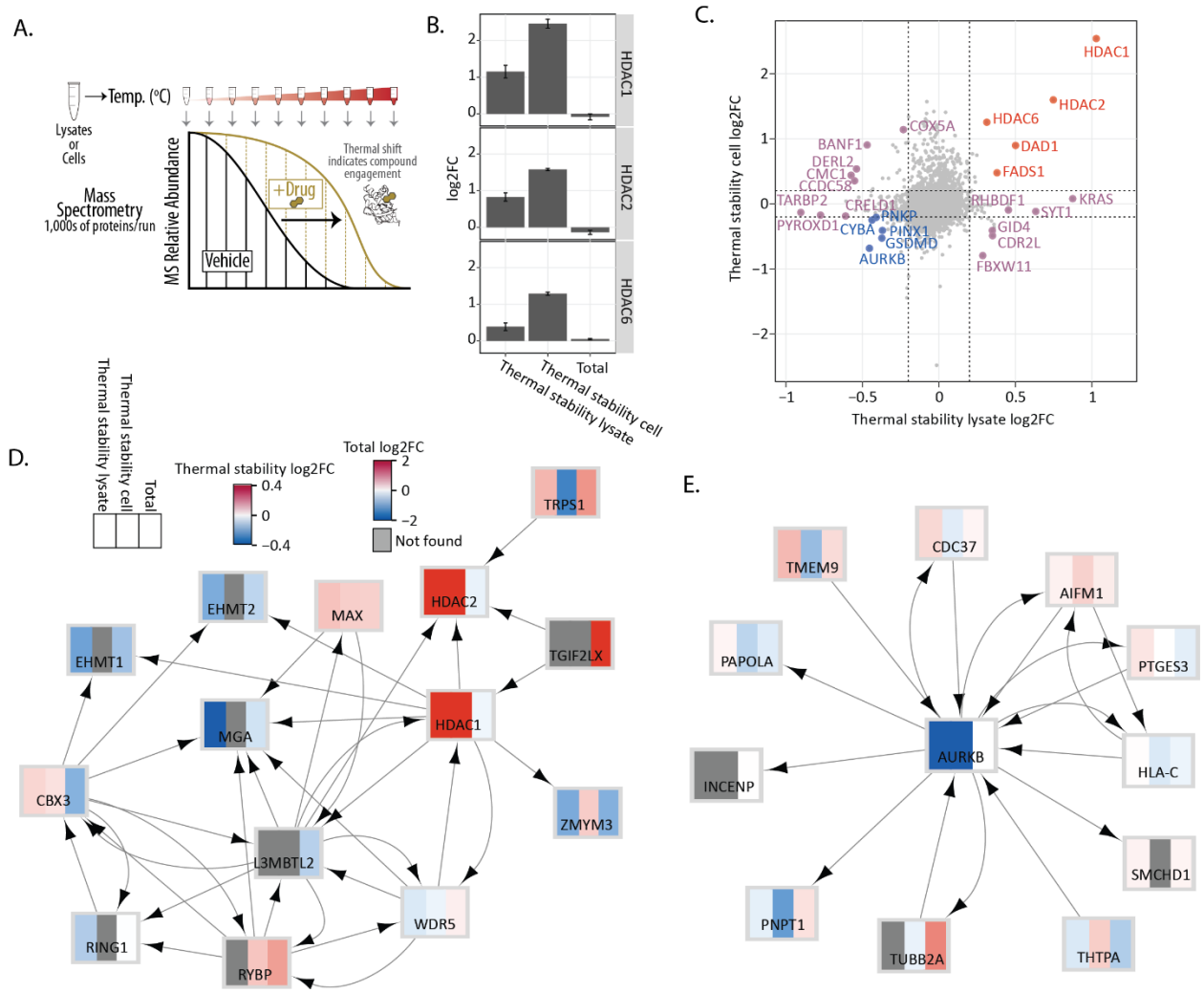

Figure 8 Analysis for protein-drug engagement for divergent cellular responses. a, Diagram of thermal stability assay. **b,** log2FC versus DMSO of HDAC1, HDAC2 and HDAC6 in two thermal stability assay and total proteomics. **c,** Activity of A549 with belinostat treatment by the protein log2FC in thermal stability assay in lysate (x-axis) and thermal stability assay in cell (y-axis). The stabilized/destabilized proteins were defined as absolute log2FC versus DMSO larger than 0.2 in thermal stability assay. **d,** Protein network of PRC1 complex. **e,** Protein network of AURKB.

Discussion

Disparate cell states within cancer cells, driven by differential genetics, signaling axis activation, and protein interactions lie at the heart of inconsistent outcome of therapeutic treatments. We chose to investigate this heterogeneity using HDAC inhibition as a model with promising preclinical anti-cancer activities, but with disputed efficacy based on cancer type and known adverse effects in clinical trials (Mamdani & Jalal, 2020). To reduce the disparities of therapeutic outcomes, we believe that it will be essential to comprehensively characterize the molecular outcomes of therapeutic intervention that represent the diversity of molecular starting points (e.g., genetic backgrounds). There are large databases characterizing different human cancer cell lines, addressing their genetic variants and cancer driver genes, such as the Cancer Cell Line Encyclopedia (CCLE). Thus, our work can add to these datasets by tracking how proteome remodeling after exposure to drug scan be leveraged to understand pre-clinical outcomes of therapeutic treatments. We combined our lung cancer specific data with recent databases describing mechanistic annotation of drugs by profiling omics data, such as DeepCoverMOA and ProteomicsDB. However, owing to the limited number of cell lines the generation of datasets that characterize how non-isogenic cell lines respond to chemical perturbation offers a new insight to understand drug mechanisms. Here, we initiate a roadmap for how lung cancer cell lines behave when they are treated with small-molecule drugs, and how this information can be used in improvement of therapeutic treatments. Importantly, we highlight that these data serve as a rich resource for hypothesis generation to determine the consequences of diverse cellular responses to small-molecule therapies.

First, we demonstrate the non-negligible differences in drug responses across various lung cancer cell lines through proteome profiling of five distinct lines. Lung cancer causes the most cancer-related deaths globally. There is emerging data regarding the genetic risks and some key oncogenes were identified, such as EGFR and KRAS (Chakravarty et al., 2017; Chang et al., 2018). However, there is not enough research about how these different oncogenes contribute to drug treatments. This dataset uncovers the relationship between cancer driver genes and drug responses. EGFR is the most common oncogene for NSCLC (LoPiccolo et al., 2024; F. Zhou & Zhou, 2018). PC9 cells have an EGFR gain of function mutant (Nagai et al., 2005), thus they are more sensitive to HDACi treatment, especially CUDC-101 which is also an EGFR inhibitor. The phosphoproteome of PC9 cells had distinct differences with other cell lines: it had more downregulated proteins than upregulated proteins, and more regulated phosphosites with HDACi treatments. In addition, the dataset also identifies unique protein expression changes corresponding to each cell line. PC9 cells had the greatest number of unique regulated proteins. However, except that the coagulation pathway was up regulated, PC9 unique regulated proteins did not concentrate in certain pathways. A549 cells had less unique regulated proteins than PC9, but these proteins were clustered in nine pathways. These unique patterns of tested cell lines with HDACi treatment can be used to predict drug performance on other untested cell lines, and further facilitate the selection of the most suitable drugs for patients with specific cancer driver genes.

Furthermore, despite the individual differences in these cell lines, we observed specific proteins consistently responding to HDACi treatments across all cell lines. Downregulated proteins were largely involved in the regulation of transcription. In addition, the JUN transcriptional factor is a key protein related to HDACi effectiveness. It was significantly upregulated in A549, H292 and

HCT116, but not regulated in PC9. Upregulation of JUN is associated with cell proliferation and differentiation (Papavassiliou & Musti, 2020), which could explain PC9 is more sensitive to HDACi. This insight helps further understand the non-canonical mechanism of action of HDACi, illustrating how these compounds alter the proteome landscape of cancer cells. The integration with PISA data also reveals potential mechanisms of HDACi, such as through the engagement of DAD1, FADS1 and AURKB. These findings together deepen our understanding of HDACi and influence their application in clinical practice.

Finally, we integrated proteomics, phosphoproteomics, transcriptomics, thermostability proteomics, and histone modification data. Integration of these data provides a comprehensive understanding of chemical regulation in cells. For example, by combining proteomics with thermal stability data and transcript profiles, we gain valuable information pertaining to the final state of the proteome but also the key drivers linking HDACi treatment to this state. Additionally, the discordant changes of transcript and protein abundance provides new insights into post-translational control of cancer cell viability, such as in the cases of CCND3, ZMYND8, ASF1B, and BRD7. For example, we note that only through the combination of transcriptomics and proteomics analyses did the zinc finger ZMYND8 become a strong candidate for future work. Thus, as we know from previous work, neither technique alone would fully recapitulate the potential mechanisms because HDACi induced increased transcript abundance but decreased protein abundance of ZMYND8. In addition, by directly profiling histone modifications in matched cells, we empowered hypothesis generation concerning a potential interaction model between ASF1B, ZMYND8 and BRD7 based on proteomics, transcriptomics, and histone proteomics. Although this dataset focuses predominantly on HDAC inhibition, extension of this multiomics approach to include more epigenetic drugs, larger cohorts of diverse cell lines, and improved methods to enhance throughput would empower our understanding of key effectors of heterogeneous molecular responses to lead compounds and established therapeutics.

Method

Cell culture conditions

A549 (CVCL_0023), H292 (CVCL_0455), HCT116 (CVCL_0291), PC9 (CVCL_B260), and PSC1 (CVCL_5622) cells were dispensed into tissue culture treated 96 well plates at a density of 37,500 cells per well in a volume of 200 µl. After 24 h, cells growing at less than 80% confluence were then treated with 10 µM of each drug, including abexinostat, belinostat, CUDC-101, trichostatin A (TSA), panobinostat, vorinostat (SAHA), and ralimetinib, or 0.1% DMSO. All treatments were performed in 6 replicates: 2 replicates for proteome analysis, 2 replicates for viability analysis and 2 replicates for BCA assay. after treatment, cells were incubated for 24 h at 37 °C before washing with 200 µl PBS per well. After all PBS was aspirated, clear cell culture plates were immediately used for sample preparation for proteomics analysis or viability assay. The viability assay was performed with CellTiter-Glo® Luminescent Cell Viability Assay (Promega).

Sample preparation for proteomics analysis

Sample lysis, reduction, alkylation, SP3 and digestion were processed with liquid handler OT2. Lysis buffer for BCA assay contains 8 M urea, 50 mM NaCl, 200 mM EPPS pH 8.5, Roche protease inhibitor tablets. Lysis buffer for proteomics analysis contains 5 mM TCEP in addition

for protein reduction. Lysis buffer 30 µl was added into each well, followed by shaking at 500 rpm for 30 min. Protein concentrations were measured using Pierce BCA assay kits. Proteins for proteomics analysis were then alkylated with 30 µl 10 mM iodoacetamide for 30 min in the dark. The alkylation reaction was quenched by adding an additional aliquot of DTT. Proteins were then transferred to a 96-well PCR plate before being isolated using SP3. In brief, 2 µl of each bead type was added to each well before adding 65 µl neat ethanol and shaking for 30 min at 1000 rpm. Samples were placed on a magnet rack and supernatant was aspirated. Beads were washed with 125 µl 80% ethanol three times by resuspending. Beads were resuspended in 40 µl digest buffer (200 mM EPPS pH 8.5, 20 ng µl-1 LysC), then incubated overnight at 37 °C with constant agitation, before adding trypsin (400 ng) for an additional 6 hr at 37 °C. The final concentration of peptide was about 1 µg/µl. Two replicates of each cell line were manually labeled with a set of TMTpro 16-plex reagents, and the mixture was incubated at room temperature for 1 h. The reaction was quenched with 0.5% hydroxylamine, before pooling beads and eluates into a single 2 ml tube and placing it on a magnetic rack. Supernatant was collected. After labeling and mixing, peptide mixtures were desalted using C18 sep-pak cartridges (50 mg, Waters).

For phosphopeptide enrichment, PureCube magnetic beads were used with modified protocol (Leutert et al., 2019). In brief, peptides were dissolved in 80% ACN, 0.1% TFA and mixed with beads, shaking for 30 min. phosphorylated peptides were eluted with 50% ACN, 2.5% NH4OH and then neutralized with 75% ACN, 10% formic acid. Elutes were desalted via Stage-tips prior to mass spectrometry analysis. Flow-throughs were then fractionated using basic-pH reverse phase chromatography (Navarrete-Perea et al., 2018). Briefly, peptides were resuspended in Buffer A (10mM ammonium bicarbonate, 5% acetonitrile, pH 8) and separated on a linear gradient from 13% to 42% Buffer B (10mM ammonium bicarbonate, 90% acetonitrile, pH 8) over an Agilent 300Extend C18 column using an Agilent 1260 HPLC equipped with wavelength detection at 214 nm and 254 nm). Fractionated peptides were desalted using Stage-tips prior to mass spectrometry analysis.

Sample preparation for protein thermal stability assay

Thermal proteome profiling (TPP) by protein integral solubility assay (PISA) was performed as previously described (Van Vranken et al., 2024). Each PISA experiment was performed in triplicate.

For live-cell PISA treatment, A549 cells were grown to a density of 1 x 10^6 cells/mL, isolated by centrifugation, and resuspended in fresh media to 6 x 10^6 cells/mL. to each well of a 24-well plate was added 500 uL of cell suspension and 1 mL of treatment (or vehicle) in media for a final cell concentration of 2x10^6 cells/mL and a final treatment concentration of 10 µM. Cells were incubated with treatment for 1 hr at room temperature. 1 mL from each incubated sample (2x10^6 cells) was collected, washed once in PBS, and resuspended in PBS containing 10 µM treatment. For each treatment condition, 30 µL of sample was aliquoted into 10 wells of a PCR plate and subjected to a temperature gradient from 48°C to 58°C for 3 minutes, then allowed to cool to room temperature for 5 minutes. 30 µL of ice-cold lysis buffer (200 mM EPPS pH 7.2, 150 mM NaCl, Roche cOmplete protease inhibitor, 0.5% NP-40) was added to each PCR plate well. 50 µL from each temperature point of a single condition was collected and pooled and cells were

allowed to lyse at 4°C for 15 minutes. Lysate was spun at maximum speed for 2 hours and the soluble fraction was collected for sample preparation for proteomic analysis.

For lysate PISA treatment, cells were resuspended in the lysis buffer as above and lysed by repeated aspiration through a 21-gauge needle. Lysate was centrifuged at maximum speed for 30 minutes at 4°C. The soluble fraction was separated, and lysate protein content was determined by BCA. Lysate and treatment were combined in lysis buffer for a final protein concentration of 1 mg/mL and a treatment concentration of 10 µM and then incubated at room temperature for 15 minutes. For each treatment condition, 30 µL of sample was aliquoted into 10 wells of a PCR plate and subjected to a temperature gradient as above. 25 µL from each temperature point of a single condition was collected, pooled, and centrifuged at maximum speed for 2 hours. The soluble fraction was collected for sample preparation for proteomic analysis.

Mass spectrometry data analysis for multiplexed quantitative proteomics

Peptides were separated prior to MS/MS analysis using an Easy-nLC (Thermo Scientific) equipped with an in-house pulled fused silica capillary column with integrated emitter packed with Accucore C18 media (Thermo Scientific). Mass spectrometric analysis was carried out on an Orbitrap Eclipse (Thermo Scientific). For whole proteome profiling, separation was carried out with 90-minute gradients from 98% Buffer A (5% ACN, 0.125% formic acid) to 28% Buffer B (90% ACN, 0.125% formic acid). Multiplexed analysis of samples was done using real-time search data acquisition (Schweppe et al., 2020), based on canonical SPS-MS3 acquisition. Briefly, a survey MS1 scan was used to identify potential peptide precursors (R = 120000, Mass range: 400-2000 m/z, max Inject time: 50ms, AGC: 200%, RF lens: 30%). The top 10 precursors were selected for fragmentation and analysis in the ion trap (Dynamic exclusion: 90s at 10 ppm, CID collision energy: 35%, max inject time: 50 ms, AGC: 200%, scan rate: rapid, isolation width: 0.5 m/z). Real-time spectral matching was carried out using the Comet search algorithm (Eng et al., 2013). If, and only if, a peptide was matched with high confidence, the instrument would then acquire an additional SPS-MS3 scan for quantification of relative abundances (R = 50000, HCD NCE: 45, max inject time: 150 ms).

For phosphopeptide profiling, separation was carried out with 90-minute gradients from 98% Buffer A (5% ACN, 0.125% formic acid) to 26% Buffer B (90% ACN, 0.125% formic acid). Multiplexed analysis of samples was done using canonical SPS-MS3 acquisition. Briefly, a survey MS1 scan was used to identify potential peptide precursors (R = 120000, Mass range: 300-2000 m/z, max Inject time: 50ms, AGC: 200%, RF lens: 30%). The top 10 precursors were selected for fragmentation and analysis in the ion trap (Dynamic exclusion: 90s at 10 ppm, HCD NCE: 30, max inject time: 35 ms, AGC: 250%, scan rate: rapid, isolation width: 0.5 m/z). SPS-MS3 was carried out in the Orbitrap (R = 50000, AGC: 250%, HCD NCE: 45, max injection time: 86 ms).

Raw spectral information was converted to mzXML format using Monocle (Rad et al., 2021), and spectra were matched using the Comet search algorithm compared against the Uniprot human database. TMTpro is a static modification at the N-terminus of peptides. The maximum missed cleavage was set as 2. Peptides and proteins were filtered to a 1% using rules of protein parsimony.

Histone extraction and LC-MS/MS analysis for HDACi treatment

The histones were extracted and prepared for chemical derivatization and digestion as described previously (Bhanu et al., 2020; Sidoli et al., 2016). Briefly, lysine residues on histones were derivatized with the propionylation reagent (1:2 reagent:sample ratio) containing acetonitrile and propionic anhydride (3:1), with the solution pH adjusted to 8.0 using ammonium hydroxide. This propionylation reaction was performed twice and the samples were then dried using a speed vac. The derivatized histones were subsequently digested with trypsin at a 1:50 ratio (wt/wt) in 50 mM ammonium bicarbonate buffer at room temperature overnight. The N-termini of histone peptides were derivatized with the propionylation reagent twice and dried on speed vac (Searfoss et al., 2023). The peptides were desalted with the self-packed C18 stage tip. After desalting, the purified peptides were dried and reconstituted in 0.1% formic acid. Peptide analysis was performed using a LC-MS/MS system consisting of a Vanquish Neo UHPLC coupled to an Orbitrap Exploris 240 (Thermo Scientific). The histone peptide samples were kept at 7 °C on sample trays during LC analysis. Separation of peptides was carried out on an Easy-Spray™ PepMap™ Neo nano-column (2 µm, C18, 75 µm X 150 mm) at room temperature with a mobile phase. The chromatography conditions consisted of a linear gradient from 2 to 32% solvent B (0.1% formic acid in 100% acetonitrile) in solvent A (0.1% formic acid in water) over 48 minutes, followed by 42 to 98% solvent B over 12 minutes, at a flow rate of 300 nL/min. The mass spectrometer was programmed for data-independent acquisition (DIA) where each acquisition cycle consisted of a full MS scan, 35 DIA MS/MS scans of 24 m/z isolation width starting from 295 m/z to reach 1100 m/z. Typically, full MS scans were acquired in the Orbitrap mass analyzer across 290–1100 m/z at a resolution of 60,000 in positive profile mode with an auto maximum injection time and an AGC target of 300%. MS/MS data from HCD fragmentation was collected in the Orbitrap. These scans typically used an NCE of 30, an AGC target of 1000%, and a maximum injection time of 60 ms. Histone MS data were analyzed with EpiProfile 2.0 (Yuan et al., 2015) .

Transcriptomics

Data regarding the HDACi-induced transcriptomic response in A549 was obtained from the NCBI GEO database under sample GSM4150378 (Srivatsan et al., 2020). Briefly, in this study, A549, MCF7, and K562 cells were treated with 4 increasing doses of a library of 188 small molecule compounds, including a subset of HDACi. The treated cells were subjected to high-throughput combinatorial indexing single-cell RNA-seq (sci-RNA-seq3). For this analysis, R package *monocle3* was used to analyze differentially expressed genes (DEGs) and for UMAP visualization (Trapnell et al., 2014; Qiu et al., 2017; J. Cao et al., 2019). For DEG analysis, the *celldataset* (cds) object was filtered to contain only A549 cells exposed to HDACi or vehicle control. For each HDACi, a generalized linear model was used to fit gene expression as a function of dose and replicate (quasi-Poisson regression) using *monocle3*'s *fit_models* function. This operation was performed on 7832 genes, determined as the union of genes expressed in 5% of cells per each inhibitor group. The p-values (Wald test) were FDR-corrected using the Benjamini-Hochberg method for multiple hypotheses, and the beta coefficients related to the contribution of dose were extracted and filtered as normalized beta coefficient > 0.05 and FDR < 5% for downstream comparison. Lastly, we performed batch integration (Haghverdi et al., 2018)

and dimensional reduction (McInnes et al., 2018) of A549 cells treated with Abexinostat, Belinostat, Panobinostat, Trichostatin A, or vehicle to visualize cellular responses to HDACi.

Data analysis

Protein quantification tables containing normalized TMT abundance ratios were analyzed with python. Coefficient of variation (CV) between replicates was calculated and filtered (CV < 0.3) before being calculated relative to DMSO. Networks were imported from BioPlex 3.0 (Schweppe et al., 2018; Huttlin et al., 2021) and modified in Cytoscape (Shannon et al., 2003).

Software used as listed:

Software	**Version**
Python	3.11.1
pandas	2.1.4
numpy	1.26.3
matplotlib	3.7.0
plotnine	0.12.4
scipy	1.11.3
statsmodels	0.14.0
PyComplexHeatmap	1.6.1
seaborn	0.13.0
gsepy	1.1.1
scikit-learn	1.3.1
Cytoscape	3.10.1
BioPlex	3.0

Data availability

For total proteomics and phosphoproteomics, 70 .RAW files have been deposited to the ProteomeXchange Consortium via the PRIDE partner repository with the data set identifier PXD051206 (Username: reviewer_pxd051206@ebi.ac.uk, password: DyNpQWlR). Spectra were searched against the human Uniprot database (download v.05/2020).

Acknowledgement

This work was supported by the following funding sources: R35GM150919-01 (D.K.S), Andy Hill CARE Foundation (D.K.S.), Cancer Consortium New Investigator Award (D.K.S).

Author contributions

C.L. and D.K.S. conceptualized the study. B.G., J.M. and D.K.S. supervised the experiments. C.L., C.S., C.M., R.K. and R.G. performed experiments. C.L. analyzed the data. C.L. drafted the original manuscript. Everyone reviewed and edited the manuscript. D.K.S. acquired funding.

Supplementary Figures

A.

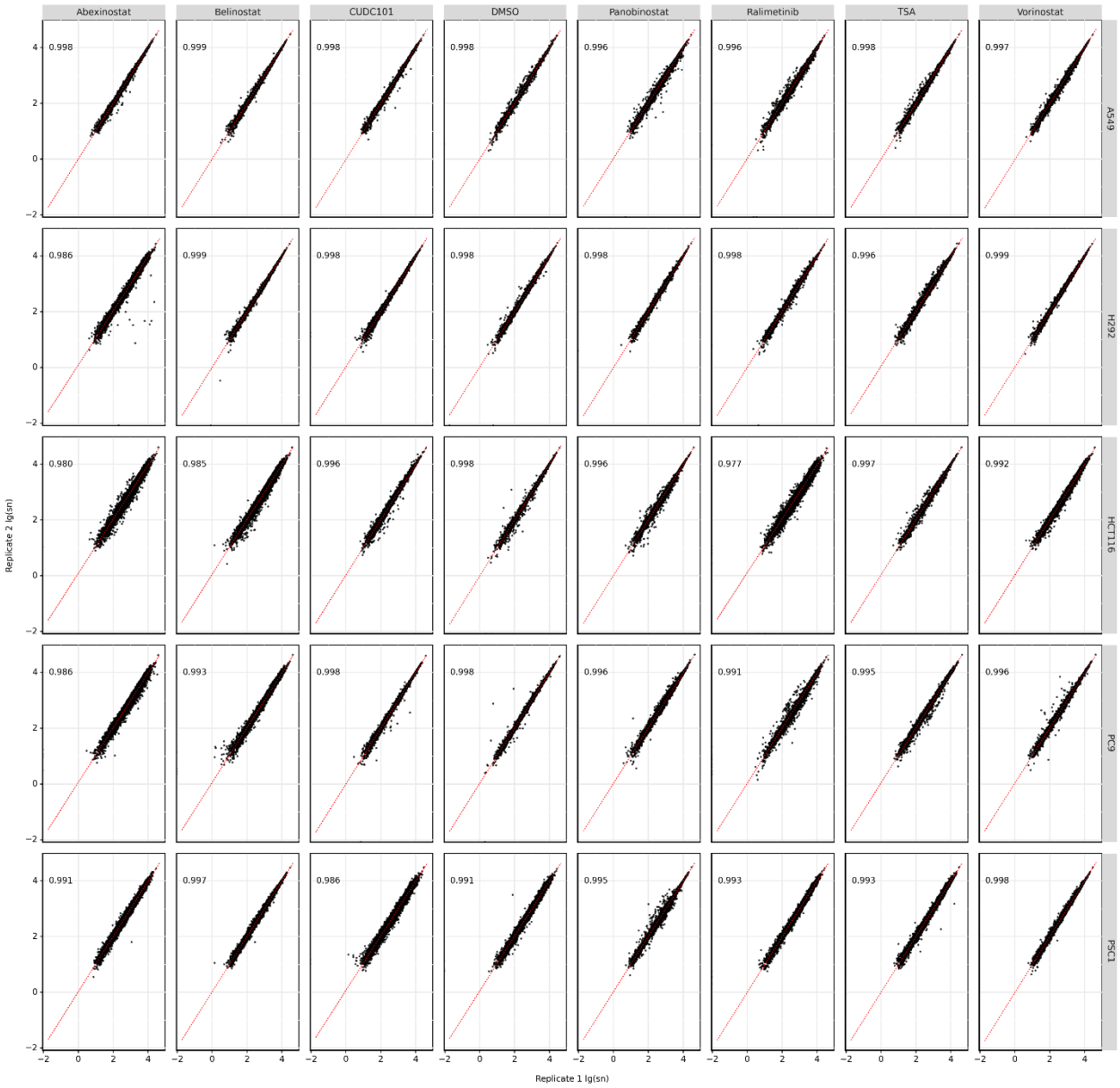

B.

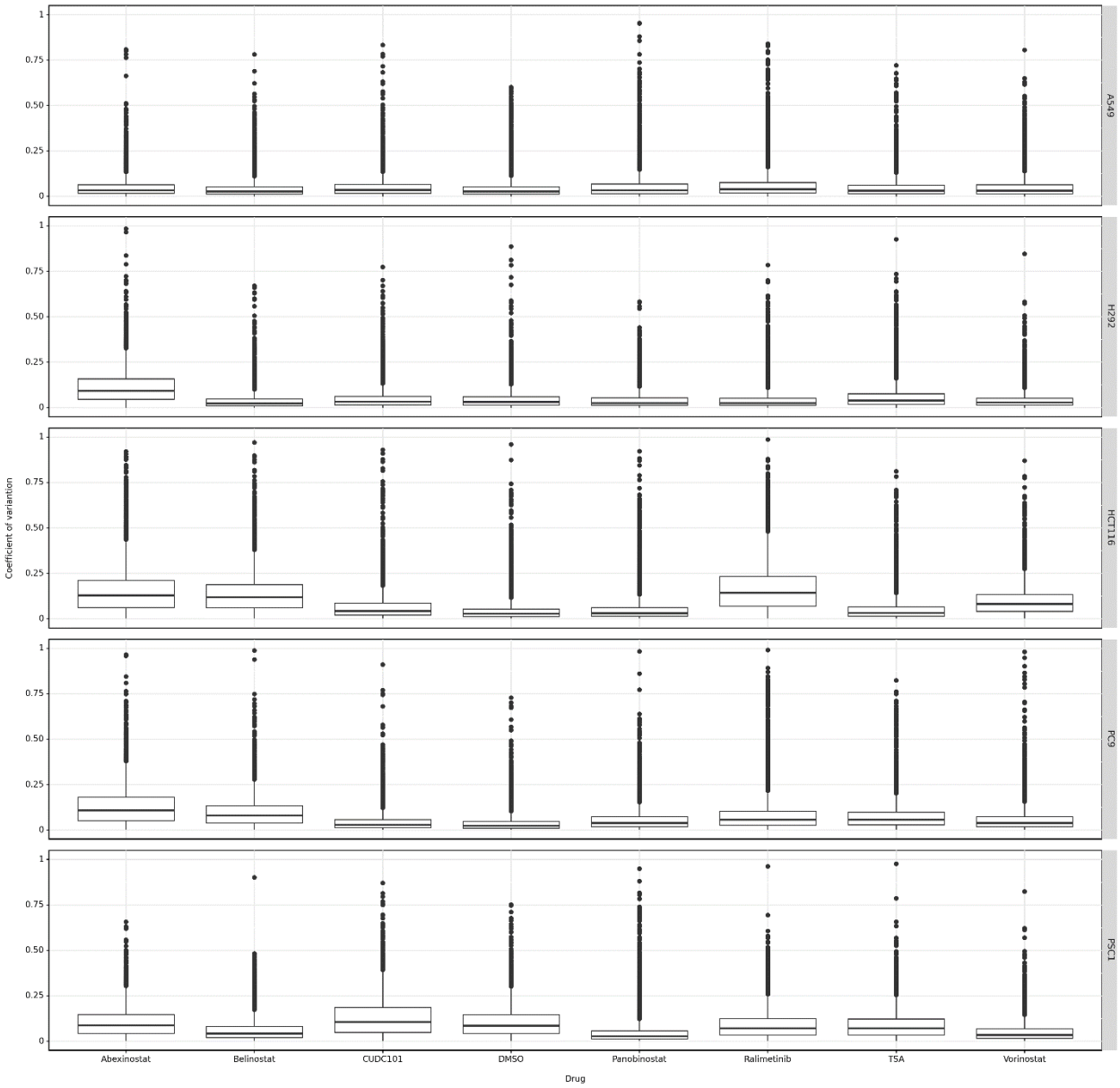

Supplementary Figure 1 Reproducibility of duplicates. a, Spearman correlation for duplicates. **b,** coefficient of variation between duplicates.

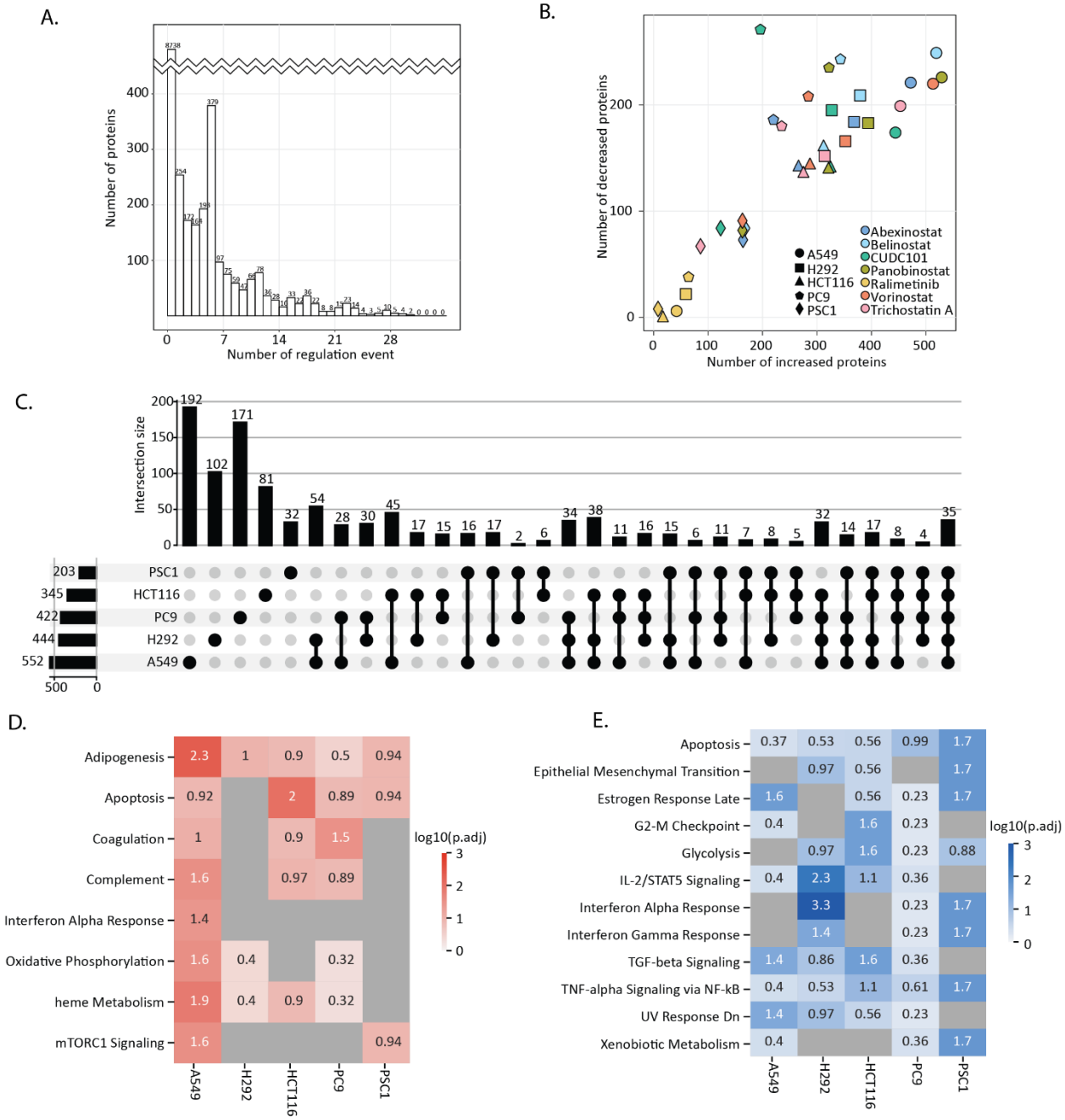

Supplementary Figure 3 Cell line specific regulation events. a, Histogram of the number of regulation events by each protein. **b,** Activity of each CXD group measured by the number of proteins down-regulated (x axis) and up-regulated (y axis) after 24 h treatment. **c,** Overlap between five lines of regulated proteins. **d,** Comparison between cell lines of Hallmark analysis of unique up-regulated proteins. **e,** Comparison between cell lines of Hallmark analysis of unique down-regulated proteins.

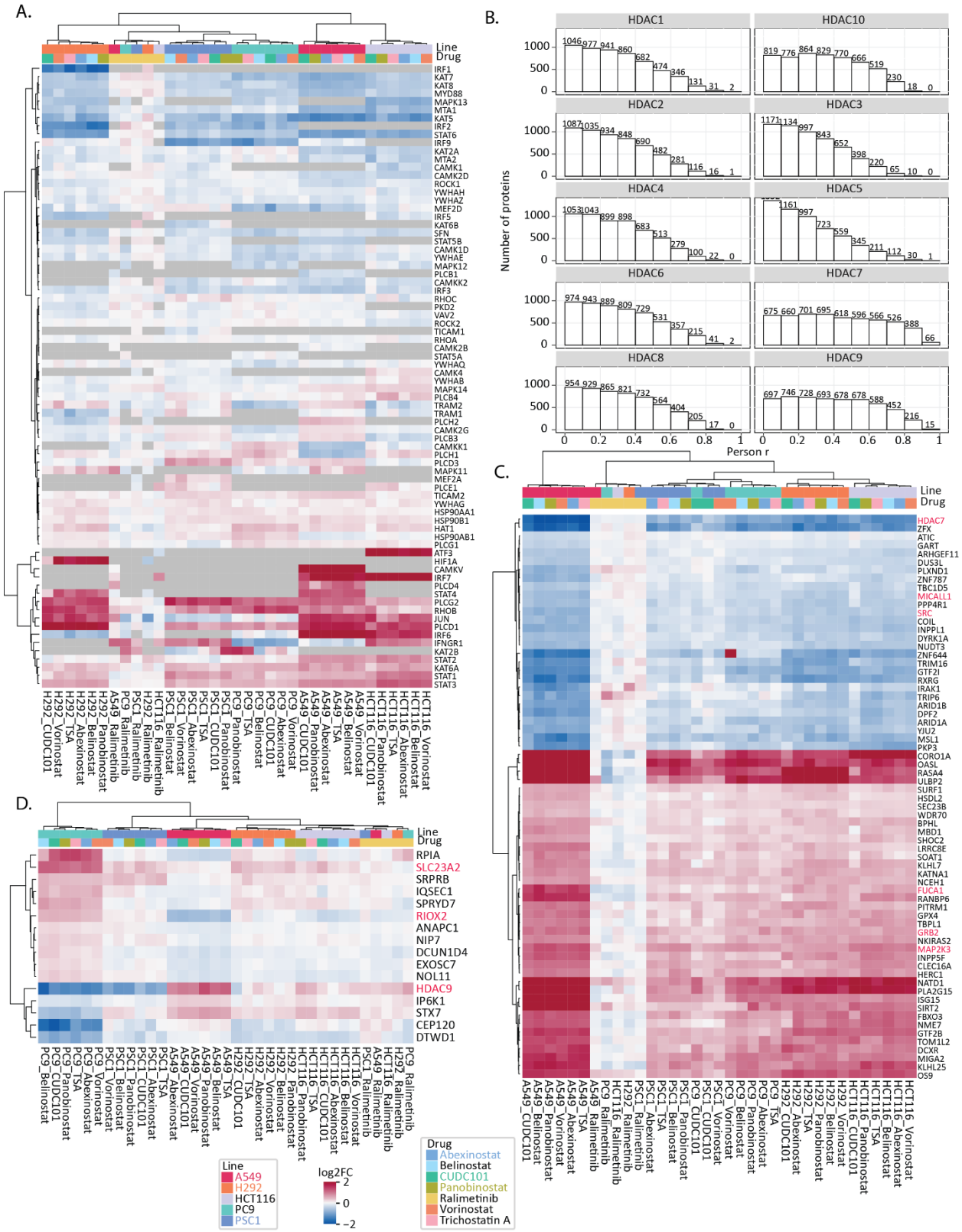

Supplementary Figure 5 Proteins correlated with HDAC7 and HDAC9. a, Heatmap of log2FC of proteins from the HDAC pathway. **b,** Number of proteins correlated with HDACs. **c,** Heatmap of log2FC of proteins correlated with HDAC7. **d,** Heatmap of log2FC of proteins

correlated with HDAC9.

A.

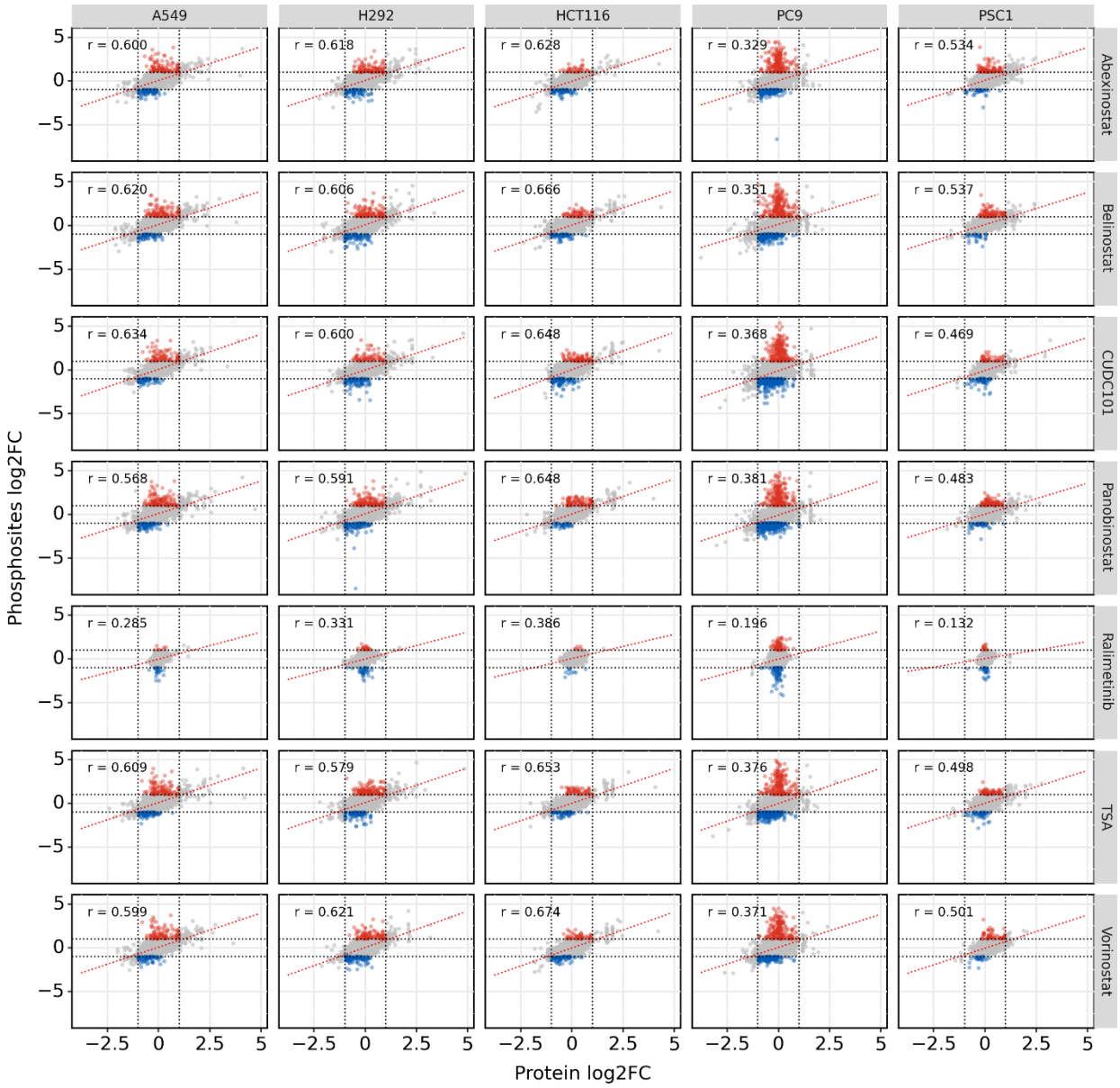

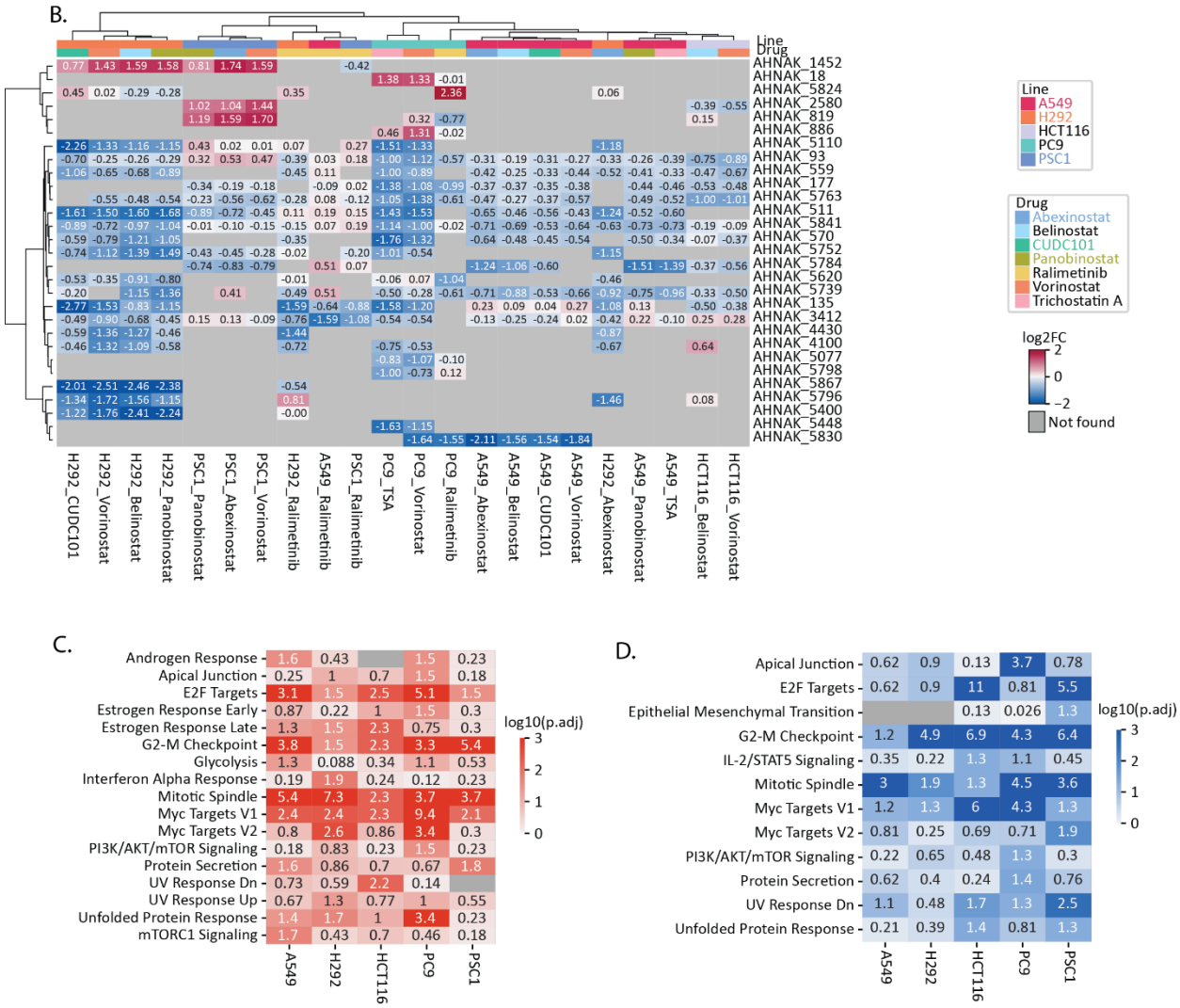

Supplementary Figure 6 Analysis of phospho-specific regulations. a, Activity of each CXD group measured by the protein log2FC (x axis) and phosphosites log2FC (y axis) after 24 h treatment. **b,** AHNAK phosphosites regulation found in some CXD groups. **c,** Hallmark analysis of proteins with phospho-specific up-regulation. **d,** Hallmark analysis of proteins with phospho-specific down-regulation.

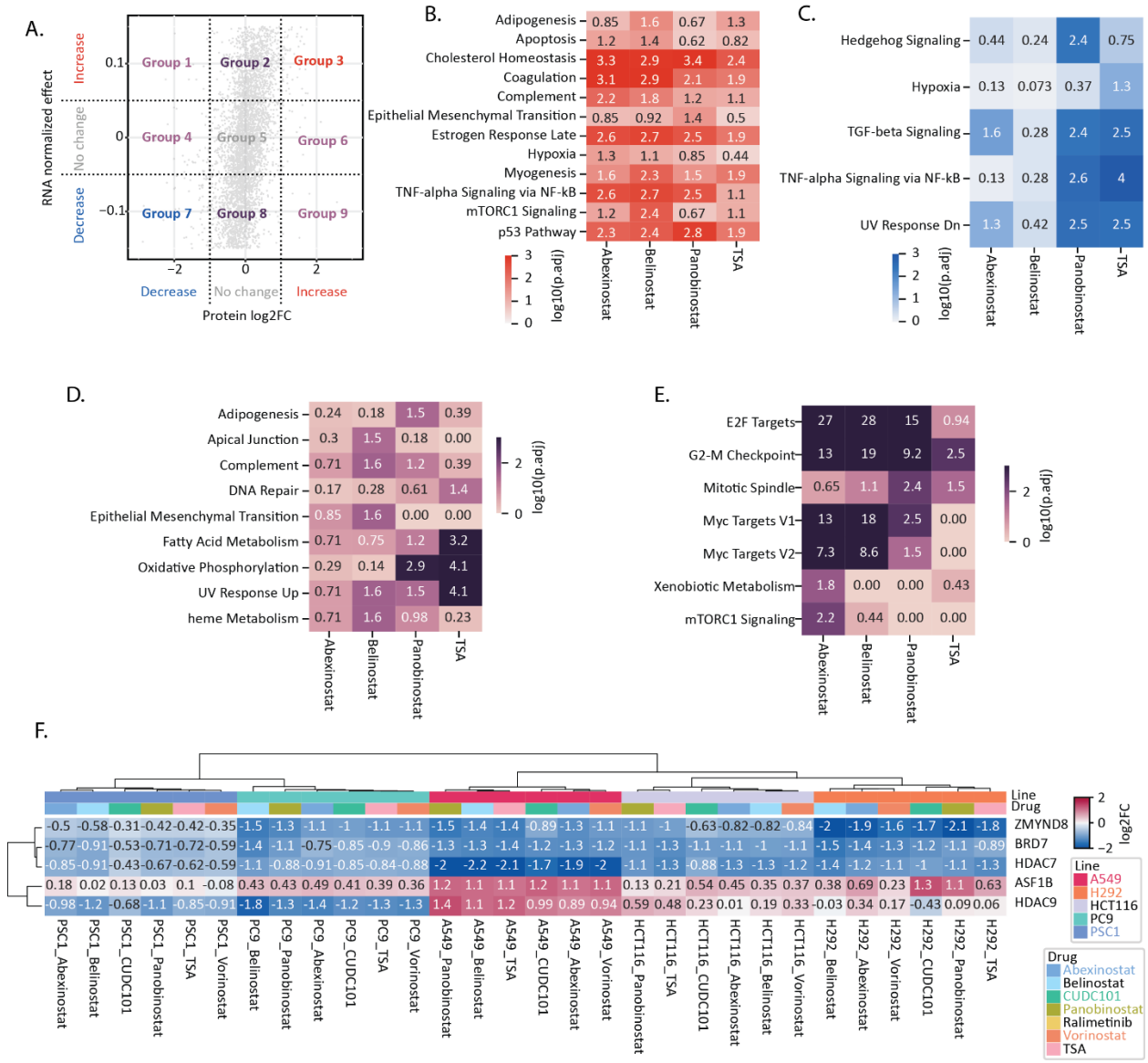

Supplementary Figure 7 Coordination between transcriptomes, proteomics and histone modification in A549 with HDACi treatments. a, Diagram shows 9 groups based on transcript and protein changes. **b,** Hallmark analysis of proteins in group 3, which were proteins up-regulated in both proteome and transcriptome datasets. **c,** Hallmark analysis of proteins in group 7, which were proteins down-regulated in both proteome and transcriptome datasets. **d,** Hallmark analysis of proteins in group 2, which were proteins not regulated in proteome but up-regulated in transcriptome datasets. **e,** Hallmark analysis of proteins in group 8, which were proteins not regulated in proteome but down-regulated transcriptome datasets. **f,** Heatmap of protein abundance changes of ASF1B, ZMYND8 and BRD7.

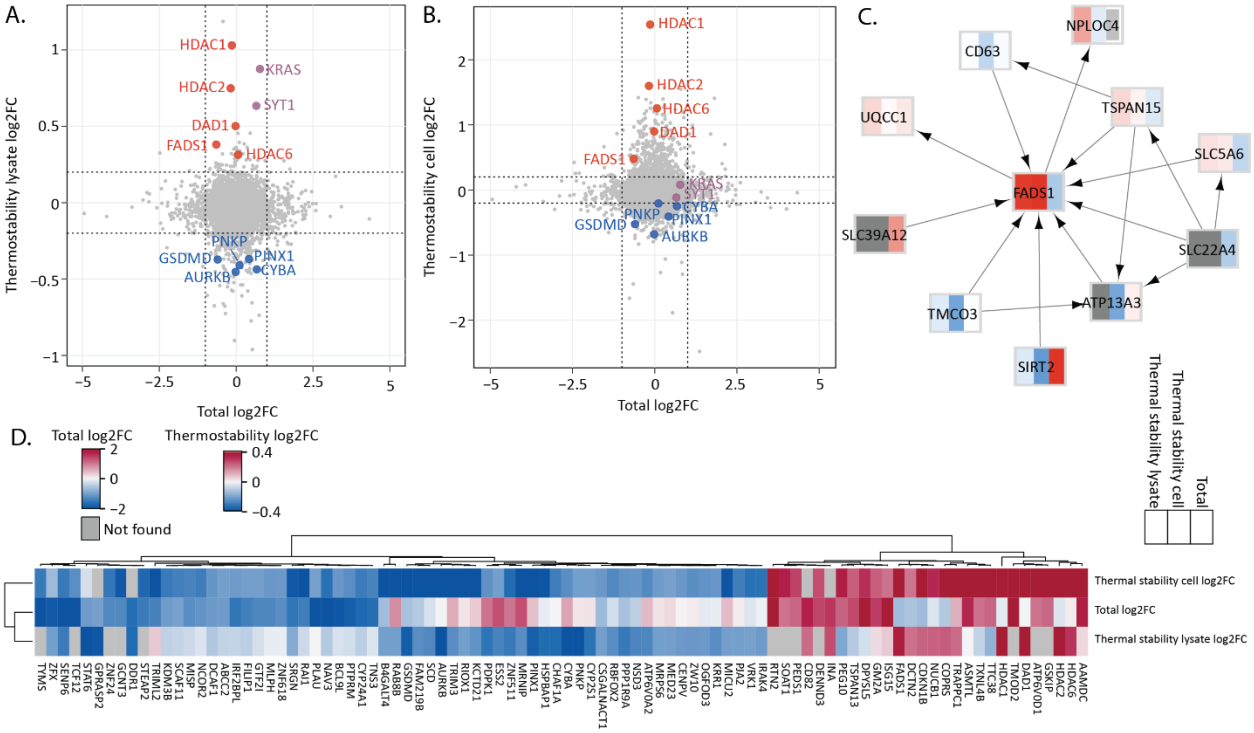

Supplementary Figure 8 Integration of thermal stability assay and total proteomics. a, Activity of A549 treated with belinostat by the protein log2FC in total proteome (x-axis) and thermostability assay in lysate (y-axis). **b,** Activity of A549 treated with belinostat by the protein log2FC in total proteome (x-axis) and thermostability assay in cell (y-axis). The regulated proteins were defined as absolute log2FC versus DMSO larger than 1 in total proteomics dataset. The stabilized/destabilized proteins were defined as absolute log2FC versus DMSO larger than 0.2 in thermostability assay. **c,** Protein network of FADS1. **d,** Heatmap of significantly regulated proteins in thermal stability assay and total proteomics.

Reference

Adhikary, S., Sanyal, S., Basu, M., Sengupta, I., Sen, S., Srivastava, D. K., Roy, S., & Das, C. (2016). Selective Recognition of H3.1K36 Dimethylation/H4K16 Acetylation Facilitates the Regulation of All-trans-retinoic Acid (ATRA)-responsive Genes by Putative Chromatin Reader ZMYND8. *The Journal of Biological Chemistry*, *291*(6), 2664–2681. https://doi.org/10.1074/jbc.M115.679985

Al-Khafaji, A. S., Davies, M. P., Risk, J. M., Marcus, M. W., Koffa, M., Gosney, J. R., Shaw, R. J., Field, J. K., & Liloglou, T. (2017). Aurora B expression modulates paclitaxel response in non-small cell lung cancer. *British Journal of Cancer*, *116*(5), 592–599. https://doi.org/10.1038/bjc.2016.453

Alvarez, F., Muñoz, F., Schilcher, P., Imhof, A., Almouzni, G., & Loyola, A. (2011). Sequential Establishment of Marks on Soluble Histones H3 and H4. *The Journal of Biological Chemistry*, *286*(20), 17714–17721. https://doi.org/10.1074/jbc.M111.223453

Bamberg, L. V., Heigwer, F., Wandmacher, A. M., Singh, A., Betge, J., Rindtorff, N., Werner, J., Josten, J., Skabkina, O. V., Hinsenkamp, I., Erdmann, G., Röcken, C., Ebert, M. P., Burgermeister, E., Zhan, T., & Boutros, M. (2022). Targeting euchromatic histone lysine methyltransferases sensitizes colorectal cancer to histone deacetylase inhibitors. *International Journal of Cancer*, *151*(9), 1586–1601. https://doi.org/10.1002/ijc.34155

Baudot, A. D., Crighton, D., O'Prey, J., Somers, J., Sierra Gonzalez, P., & Ryan, K. M. (2016). P53 directly regulates the glycosidase FUCA1 to promote chemotherapy-induced cell death. *Cell Cycle*, *15*(17), 2299–2308. https://doi.org/10.1080/15384101.2016.1191714

Begley, C. G., & Ellis, L. M. (2012). Raise standards for preclinical cancer research. *Nature*, *483*(7391), 531–533. https://doi.org/10.1038/483531a

Bhanu, N. V., Sidoli, S., & Garcia, B. A. (2020). A Workflow for Ultra-rapid Analysis of Histone Post-translational Modifications with Direct-injection Mass Spectrometry. *Bio-Protocol*, *10*(18), e3756. https://doi.org/10.21769/BioProtoc.3756

Blaj, C., Bringmann, A., Schmidt, E. M., Urbischek, M., Lamprecht, S., Fröhlich, T., Arnold, G. J., Krebs, S., Blum, H., Hermeking, H., Jung, A., Kirchner, T., & Horst, D. (2017). ADNP Is a Therapeutically Inducible Repressor of WNT Signaling in Colorectal Cancer. *Clinical Cancer Research*, *23*(11), 2769–2780. https://doi.org/10.1158/1078-0432.CCR-16-1604

Bockstaele, L., Kooken, H., Libert, F., Paternot, S., Dumont, J. E., de Launoit, Y., Roger, P. P., & Coulonval, K. (2006). Regulated Activating Thr172 Phosphorylation of Cyclin-Dependent Kinase 4(CDK4): Its Relationship with Cyclins and CDK "Inhibitors." *Molecular and Cellular Biology*, *26*(13), 5070–5085. https://doi.org/10.1128/MCB.02006-05

Cao, J., Spielmann, M., Qiu, X., Huang, X., Ibrahim, D. M., Hill, A. J., Zhang, F., Mundlos, S., Christiansen, L., Steemers, F. J., Trapnell, C., & Shendure, J. (2019). The single-cell transcriptional landscape of mammalian organogenesis. *Nature*, *566*(7745), 496–502. https://doi.org/10.1038/s41586-019-0969-x

Cao, X. X., Mohuiddin, I., Ece, F., McConkey, D. J., & Smythe, W. R. (2001). Histone Deacetylase Inhibitor Downregulation of bcl-xl Gene Expression Leads to Apoptotic Cell Death in Mesothelioma. *American Journal of Respiratory Cell and Molecular Biology*, *25*(5), 562–568. https://doi.org/10.1165/ajrcmb.25.5.4539

Chakravarty, D., Gao, J., Phillips, S. M., Kundra, R., Zhang, H., Wang, J., Rudolph, J. E., Yaeger, R., Soumerai, T., Nissan, M. H., Chang, M. T., Chandarlapaty, S., Traina, T. A., Paik, P. K., Ho, A. L., Hantash, F. M., Grupe, A., Baxi, S. S., Callahan, M. K., … Schultz, N. (2017). OncoKB: A Precision Oncology Knowledge Base. *JCO Precision Oncology*, *2017*, PO.17.00011. https://doi.org/10.1200/PO.17.00011

Chang, M. T., Bhattarai, T. S., Schram, A. M., Bielski, C. M., Donoghue, M. T. A., Jonsson, P., Chakravarty, D., Phillips, S., Kandoth, C., Penson, A., Gorelick, A., Shamu, T., Patel, S., Harris, C., Gao, J., Sumer, S. O., Kundra, R., Razavi, P., Li, B. T., … Taylor, B. S. (2018). Accelerating Discovery of Functional Mutant Alleles in Cancer. *Cancer Discovery*, *8*(2), 174–183. https://doi.org/10.1158/2159-8290.CD-17-0321

Chittock, E. C., Latwiel, S., Miller, T. C. R., & Müller, C. W. (2017). Molecular architecture of polycomb repressive complexes. *Biochemical Society Transactions*, *45*(1), 193–205. https://doi.org/10.1042/BST20160173

Cong, P., Jie, Z., Ying, L. H., Ming, Z., Li, W. L., Hong, Z. Q., Xin, Y. Y., Wei, X., Rong, S. S., Ling, L. X., & Yuan, L. G. (2006). The transcriptional regulation role of BRD7 by binding to acetylated histone through bromodomain. *Journal of Cellular Biochemistry*, *97*(4), 882–892. https://doi.org/10.1002/jcb.20645

Daniels, R. H., & Bokoch, G. M. (1999). p21-Activated protein kinase: A crucial component of morphological signaling? *Trends in Biochemical Sciences*, *24*(9), 350–355. https://doi.org/10.1016/S0968-0004(99)01442-5

Davis, T. A., Loos, B., & Engelbrecht, A.-M. (2014). AHNAK: The giant jack of all trades. *Cellular Signalling*, *26*(12), 2683–2693. https://doi.org/10.1016/j.cellsig.2014.08.017

Ding, C., Tang, W., Wu, H., Fan, X., Luo, J., Feng, J., Wen, K., & Wu, G. (2019). The PEAK1–PPP1R12B axis inhibits tumor growth and metastasis by regulating Grb2/PI3K/Akt signalling in colorectal cancer. *Cancer Letters*, *442*, 383–395. https://doi.org/10.1016/j.canlet.2018.11.014

Duell, E. J., Lujan-Barroso, L., Llivina, C., Muñoz, X., Jenab, M., Boutron-Ruault, M.-C., Clavel-Chapelon, F., Racine, A., Boeing, H., Buijsse, B., Canzian, F., Johnson, T., Dalgård, C., Overvad, K., Tjønneland, A., Olsen, A., Sánchez, S. C., Sánchez-Cantalejo, E., Huerta, J.-M., … González, C. A. (2013). Vitamin C transporter gene (SLC23A1 and SLC23A2) polymorphisms, plasma vitamin C levels, and gastric cancer risk in the EPIC cohort. *Genes & Nutrition*, *8*(6), 549–560. https://doi.org/10.1007/s12263-013-0346-6

Dymova, M. A., Vasileva, N. S., Kuligina, E. V., Savinovskaya, Y. I., Zinchenko, N. D., Ageenko, A. B., Mishinov, S. V., Stepanov, G. A., Richter, V. A., & Semenov, D. V. (2022). MicroRNA and mRNA Expression Changes in Glioblastoma Cells Cultivated under Conditions of Neurosphere Formation. *Current Issues in Molecular Biology*, *44*(11), Article 11. https://doi.org/10.3390/cimb44110360

Eng, J. K., Jahan, T. A., & Hoopmann, M. R. (2013). Comet: An open-source MS/MS sequence database search tool. *PROTEOMICS*, *13*(1), 22–24. https://doi.org/10.1002/pmic.201200439

Fandy, T. E., & Srivastava, R. K. (2006). Trichostatin A sensitizes TRAIL-resistant myeloma cells by downregulation of the antiapoptotic Bcl-2 proteins. *Cancer Chemotherapy and Pharmacology*, *58*(4), 471–477. https://doi.org/10.1007/s00280-005-0184-3

Gaetani, M., Sabatier, P., Saei, A. A., Beusch, C. M., Yang, Z., Lundström, S. L., & Zubarev, R. A. (2019). Proteome Integral Solubility Alteration: A High-Throughput Proteomics Assay for Target Deconvolution. *Journal of Proteome Research*, *18*(11), 4027–4037. https://doi.org/10.1021/acs.jproteome.9b00500

Gajewski, T. F., & Thompson, C. B. (1996). Apoptosis Meets Signal Transduction: Elimination of a BAD Influence. *Cell*, *87*(4), 589–592. https://doi.org/10.1016/S0092-8674(00)81377-X

Glass, D. B., el-Maghrabi, M. R., & Pilkis, S. J. (1986). Synthetic peptides corresponding to the site phosphorylated in 6-phosphofructo-2-kinase/fructose-2,6-bisphosphatase as substrates of cyclic nucleotide-dependent protein kinases. *The Journal of Biological Chemistry*, *261*(6), 2987–2993.

Glass, D. B., & Smith, S. B. (1983). Phosphorylation by cyclic GMP-dependent protein kinase of a synthetic peptide corresponding to the autophosphorylation site in the enzyme. *The Journal of Biological Chemistry*, *258*(24), 14797–14803.

Govers, A. M. A. P., Wiggers, C. R. M., van Boxtel, R., Mokry, M., Nieuwenhuis, E. E. S., Creyghton, M. P., Bartels, M., & Coffer, P. J. (2019). Transcriptomic and Epigenomic Profiling of Histone Deacetylase Inhibitor Treatment Reveals Distinct Gene Regulation Profiles Leading to Impaired Neutrophil Development. *HemaSphere*, *3*(4), e270. https://doi.org/10.1097/HS9.0000000000000270

Haghverdi, L., Lun, A. T. L., Morgan, M. D., & Marioni, J. C. (2018). Batch effects in single-cell RNA sequencing data are corrected by matching mutual nearest neighbours. *Nature Biotechnology*, *36*(5), 421–427. https://doi.org/10.1038/nbt.4091

Hakimi, M.-A., Dong, Y., Lane, W. S., Speicher, D. W., & Shiekhattar, R. (2003). A Candidate X-linked Mental Retardation Gene Is a Component of a New Family of Histone Deacetylase-containing Complexes *. *Journal of Biological Chemistry*, *278*(9), 7234–7239. https://doi.org/10.1074/jbc.M208992200

Hayashi, A., Horiuchi, A., Kikuchi, N., Hayashi, T., Fuseya, C., Suzuki, A., Konishi, I., & Shiozawa, T. (2010). Type-specific roles of histone deacetylase (HDAC) overexpression in ovarian carcinoma: HDAC1 enhances cell proliferation and HDAC3 stimulates cell migration with downregulation of E-cadherin. *International Journal of Cancer*, *127*(6), 1332–1346. https://doi.org/10.1002/ijc.25151

Hirsch, C. L., Smith-Windsor, E. L., & Bonham, K. (2006). Src family kinase members have a common response to histone deacetylase inhibitors in human colon cancer cells. *International Journal of Cancer*, *118*(3), 547–554. https://doi.org/10.1002/ijc.21383

Hu, K., Wu, W., Li, Y., Lin, L., Chen, D., Yan, H., Xiao, X., Chen, H., Chen, Z., Zhang, Y., Xu, S., Guo, Y., Koeffler, H. P., Song, E., & Yin, D. (2019). Poly(ADP-ribosyl)ation of BRD7 by PARP1 confers resistance to DNA-damaging chemotherapeutic agents. *EMBO Reports*, *20*(5), e46166. https://doi.org/10.15252/embr.201846166

Huang, Z., Xia, Y., Hu, K., Zeng, S., Wu, L., Liu, S., Zhi, C., Lai, M., Chen, D., Xie, L., & Yuan, Z. (2020). Histone deacetylase 6 promotes growth of glioblastoma through the MKK7/JNK/c-Jun signaling pathway. *Journal of Neurochemistry*, *152*(2), 221–234. https://doi.org/10.1111/jnc.14849

Huttlin, E. L., Bruckner, R. J., Navarrete-Perea, J., Cannon, J. R., Baltier, K., Gebreab, F., Gygi, M. P., Thornock, A., Zarraga, G., Tam, S., Szpyt, J., Gassaway, B. M., Panov, A., Parzen, H., Fu, S., Golbazi, A., Maenpaa, E., Stricker, K., Guha Thakurta, S., … Gygi, S. P. (2021). Dual proteome-scale networks reveal cell-specific remodeling of the human interactome. *Cell*, *184*(11), 3022-3040.e28. https://doi.org/10.1016/j.cell.2021.04.011

Inoue, A., & Fujimoto, D. (1969). Enzymatic deacetylation of histone. *Biochemical and Biophysical Research Communications*, *36*(1), 146–150. https://doi.org/10.1016/0006-291x(69)90661-5

Jin, Z., Jiang, W., Jiao, F., Guo, Z., Hu, H., Wang, L., & Wang, L. (2014). Decreased expression of histone deacetylase 10 predicts poor prognosis of gastric cancer patients. *International Journal of Clinical and Experimental Pathology*, *7*(9), 5872–5879.

Jung, K. H., Noh, J. H., Kim, J. K., Eun, J. W., Bae, H. J., Chang, Y. G., Kim, M. G., Park, W. S., Lee, J. Y., Lee, S.-Y., Chu, I.-S., & Nam, S. W. (2012). Histone deacetylase 6 functions as a tumor suppressor by activating c-Jun NH2-terminal kinase-mediated beclin 1-dependent autophagic cell death in liver cancer. *Hepatology*, *56*(2), 644–657. https://doi.org/10.1002/hep.25699

Jung, K. H., Noh, J. H., Kim, J. K., Eun, J. W., Bae, H. J., Xie, H. J., Chang, Y. G., Kim, M. G., Park, H., Lee, J. Y., & Nam, S. W. (2012). HDAC2 overexpression confers oncogenic potential to human lung cancer cells by deregulating expression of apoptosis and cell cycle proteins. *Journal of Cellular Biochemistry*, *113*(6), 2167–2177. https://doi.org/10.1002/jcb.24090

Kiweler, N., Wünsch, D., Wirth, M., Mahendrarajah, N., Schneider, G., Stauber, R. H., Brenner, W., Butter, F., & Krämer, O. H. (2020). Histone deacetylase inhibitors dysregulate DNA repair proteins and antagonize metastasis-associated processes. *Journal of Cancer Research and Clinical Oncology*, *146*(2), 343–356. https://doi.org/10.1007/s00432-019-03118-4

Komiya, K., Sueoka-Aragane, N., Sato, A., Hisatomi, T., Sakuragi, T., Mitsuoka, M., Sato, T., Hayashi, S., Izumi, H., Tsuneoka, M., & Sueoka, E. (2010). Mina53, a novel c-Myc target gene, is frequently expressed in lung cancers and exerts oncogenic property in NIH/3T3 cells. *Journal of Cancer Research and Clinical Oncology*, *136*(3), 465–473. https://doi.org/10.1007/s00432-009-0679-0

Kwak, S.-M., Seo, J., Hwang, J.-T., Sung, G.-J., Song, J.-H., Jeong, J.-H., Lee, S.-H., Yoon, H.-G., Choi, H.-K., & Choi, K.-C. (2019). EGFR–c-Src-Mediated HDAC3 Phosphorylation Exacerbates Invasion of Breast Cancer Cells. *Cells*, *8*(8), Article 8. https://doi.org/10.3390/cells8080930

LaBaer, J., Garrett, M. D., Stevenson, L. F., Slingerland, J. M., Sandhu, C., Chou, H. S., Fattaey, A., & Harlow, E. (1997). New functional activities for the p21 family of CDK inhibitors. *Genes & Development*, *11*(7), 847–862. https://doi.org/10.1101/gad.11.7.847

Leon, C., Manley, E., Neely, A. M., Castillo, J., Ramos Correa, M., Velarde, D. A., Yang, M., Puente, P. E., Romero, D. I., Ren, B., Chai, W., Gladstone, M., Lamango, N. S., Huang, Y., & Offringa, I. A. (2023). Lack of racial and ethnic diversity in lung cancer cell lines contributes to lung cancer health disparities. *Frontiers in Oncology*, *13*. https://www.frontiersin.org/articles/10.3389/fonc.2023.1187585

Leung, J. W. C., Makharashvili, N., Agarwal, P., Chiu, L.-Y., Pourpre, R., Cammarata, M. B., Cannon, J. R., Sherker, A., Durocher, D., Brodbelt, J. S., Paull, T. T., & Miller, K. M. (2017). ZMYM3 regulates BRCA1 localization at damaged chromatin to promote DNA repair. *Genes & Development*, *31*(3), 260–274. https://doi.org/10.1101/gad.292516.116

Leutert, M., Rodríguez-Mias, R. A., Fukuda, N. K., & Villén, J. (2019). R2-P2 rapid-robotic phosphoproteomics enables multidimensional cell signaling studies. *Molecular Systems Biology*, *15*(12), e9021. https://doi.org/10.15252/msb.20199021

Li, N., Li, Y., Lv, J., Zheng, X., Wen, H., Shen, H., Zhu, G., Chen, T.-Y., Dhar, S. S., Kan, P.-Y., Wang, Z., Shiekhattar, R., Shi, X., Lan, F., Chen, K., Li, W., Li, H., & Lee, M. G. (2016). ZMYND8 reads the dual histone mark H3K4me1-H3K14ac to antagonize the expression of metastasis-linked genes. *Molecular Cell*, *63*(3), 470–484. https://doi.org/10.1016/j.molcel.2016.06.035

Li, Y., & Seto, E. (2016). HDACs and HDAC Inhibitors in Cancer Development and Therapy. *Cold Spring Harbor Perspectives in Medicine*, *6*(10), a026831. https://doi.org/10.1101/cshperspect.a026831

Li, Z., Huang, J., Yuan, H., Chen, Z., Luo, Q., & Lu, S. (2016). SIRT2 inhibits non-small cell lung cancer cell growth through impairing Skp2-mediated p27 degradation. *Oncotarget*, *7*(14), 18927–18939. https://doi.org/10.18632/oncotarget.7816

Liberzon, A., Birger, C., Thorvaldsdóttir, H., Ghandi, M., Mesirov, J. P., & Tamayo, P. (2015). The Molecular Signatures Database (MSigDB) hallmark gene set collection. *Cell Systems*, *1*(6), 417–425. https://doi.org/10.1016/j.cels.2015.12.004

Liu, X., Song, J., Zhang, Y., Wang, H., Sun, H., Feng, X., Hou, M., Chen, G., Tang, Q., & Ji, M. (2020). ASF1B promotes cervical cancer progression through stabilization of CDK9. *Cell Death & Disease*, *11*(8), 1–15. https://doi.org/10.1038/s41419-020-02872-5

Liu, Y.-L., Yang, P.-M., Shun, C.-T., Wu, M.-S., Weng, J.-R., & Chen, C.-C. (2010). Autophagy potentiates the anti-cancer effects of the histone

deacetylase inhibitors in hepatocellular carcinoma. *Autophagy*, *6*(8), 1057–1065. https://doi.org/10.4161/auto.6.8.13365
Longworth, M. S., & Laimins, L. A. (2006). Histone deacetylase 3 localizes to the plasma membrane and is a substrate of Src. *Oncogene*, *25*(32), Article 32. https://doi.org/10.1038/sj.onc.1209473
LoPiccolo, J., Gusev, A., Christiani, D. C., & Jänne, P. A. (2024). Lung cancer in patients who have never smoked—An emerging disease. *Nature Reviews Clinical Oncology*, *21*(2), 121–146. https://doi.org/10.1038/s41571-023-00844-0
Lowenstein, E. J., Daly, R. J., Batzer, A. G., Li, W., Margolis, B., Lammers, R., Ullrich, A., Skolnik, E. Y., Bar-Sagi, D., & Schlessinger, J. (1992). The SH2 and SH3 domain-containing protein GRB2 links receptor tyrosine kinases to ras signaling. *Cell*, *70*(3), 431–442. https://doi.org/10.1016/0092-8674(92)90167-b
Lv, Z., Weng, X., Du, C., Zhang, C., Xiao, H., Cai, X., Ye, S., Cheng, J., Ding, C., Xie, H., Zhou, L., Wu, J., & Zheng, S. (2016). Downregulation of HDAC6 promotes angiogenesis in hepatocellular carcinoma cells and predicts poor prognosis in liver transplantation patients. *Molecular Carcinogenesis*, *55*(5), 1024–1033. https://doi.org/10.1002/mc.22345
Ma, C., & D'Mello, S. R. (2011). Neuroprotection by Histone Deacetylase-7 (HDAC7) Occurs by Inhibition of c-jun Expression through a Deacetylase-independent Mechanism. *The Journal of Biological Chemistry*, *286*(6), 4819–4828. https://doi.org/10.1074/jbc.M110.146860
Maeda, T., Towatari, M., Kosugi, H., & Saito, H. (2000). Up-regulation of costimulatory/adhesion molecules by histone deacetylase inhibitors in acute myeloid leukemia cells. *Blood*, *96*(12), 3847–3856. https://doi.org/10.1182/blood.V96.12.3847
Magner, W. J., Kazim, A. L., Stewart, C., Romano, M. A., Catalano, G., Grande, C., Keiser, N., Santaniello, F., & Tomasi, T. B. (2000). Activation of MHC Class I, II, and CD40 Gene Expression by Histone Deacetylase Inhibitors1. *The Journal of Immunology*, *165*(12), 7017–7024. https://doi.org/10.4049/jimmunol.165.12.7017
Majumdar, G., Adris, P., Bhargava, N., Chen, H., & Raghow, R. (2012). Pan-histone deacetylase inhibitors regulate signaling pathways involved in proliferative and pro-inflammatory mechanisms in H9c2 cells. *BMC Genomics*, *13*(1), 709. https://doi.org/10.1186/1471-2164-13-709
Mamdani, H., & Jalal, S. I. (2020). Histone Deacetylase Inhibition in Non-small Cell Lung Cancer: Hype or Hope? *Frontiers in Cell and Developmental Biology*, *8*. https://www.frontiersin.org/articles/10.3389/fcell.2020.582370
Mann, B. S., Johnson, J. R., Cohen, M. H., Justice, R., & Pazdur, R. (2007). FDA Approval Summary: Vorinostat for Treatment of Advanced Primary Cutaneous T-Cell Lymphoma. *The Oncologist*, *12*(10), 1247–1252. https://doi.org/10.1634/theoncologist.12-10-1247
Matteucci, E., Ridolfi, E., Maroni, P., Bendinelli, P., & Desiderio, M. A. (2007). C-Src/Histone Deacetylase 3 Interaction Is Crucial for Hepatocyte Growth Factor–Dependent Decrease of CXCR4 Expression in Highly Invasive Breast Tumor Cells. *Molecular Cancer Research*, *5*(8), 833–845. https://doi.org/10.1158/1541-7786.MCR-07-0054
McDermott, J., & Jimeno, A. (2014). Belinostat for the treatment of peripheral T-cell lymphomas. *Drugs of Today (Barcelona, Spain*, *50*(5), 337–345. https://doi.org/10.1358/dot.2014.50.5.2138703
McInnes, L., Healy, J., Saul, N., & Großberger, L. (2018). UMAP: Uniform Manifold Approximation and Projection. *Journal of Open Source Software*, *3*(29), 861. https://doi.org/10.21105/joss.00861
Melhuish, T. A., Gallo, C. M., & Wotton, D. (2001). TGIF2 Interacts with Histone Deacetylase 1 and Represses Transcription *. *Journal of Biological Chemistry*, *276*(34), 32109–32114. https://doi.org/10.1074/jbc.M103377200
Minamiya, Y., Ono, T., Saito, H., Takahashi, N., Ito, M., Mitsui, M., Motoyama, S., & Ogawa, J. (2011). Expression of histone deacetylase 1 correlates with a poor prognosis in patients with adenocarcinoma of the lung. *Lung Cancer*, *74*(2), 300–304. https://doi.org/10.1016/j.lungcan.2011.02.019
Minamiya, Y., Ono, T., Saito, H., Takahashi, N., Ito, M., Motoyama, S., & Ogawa, J. (2010). Strong expression of HDAC3 correlates with a poor prognosis in patients with adenocarcinoma of the lung. *Tumor Biology*, *31*(5), 533–539. https://doi.org/10.1007/s13277-010-0066-0
Mitchell, D. C., Kuljanin, M., Li, J., Van Vranken, J. G., Bulloch, N., Schweppe, D. K., Huttlin, E. L., & Gygi, S. P. (2023). A proteome-wide atlas of drug mechanism of action. *Nature Biotechnology*. https://doi.org/10.1038/s41587-022-01539-0
Miyanaga, A., Gemma, A., Noro, R., Kataoka, K., Matsuda, K., Nara, M., Okano, T., Seike, M., Yoshimura, A., Kawakami, A., Uesaka, H., Nakae, H., & Kudoh, S. (2008). Antitumor activity of histone deacetylase inhibitors in non-small cell lung cancer cells: Development of a molecular predictive model. *Molecular Cancer Therapeutics*, *7*(7), 1923–1930. https://doi.org/10.1158/1535-7163.MCT-07-2140
Morrison, B. E., Majdzadeh, N., Zhang, X., Lyles, A., Bassel-Duby, R., Olson, E. N., & D'Mello, S. R. (2006). Neuroprotection by Histone Deacetylase-Related Protein. *Molecular and Cellular Biology*, *26*(9), 3550–3564. https://doi.org/10.1128/MCB.26.9.3550-3564.2006
Mukherjee, S., Sen, S., Adhikary, S., Sengupta, A., Mandal, P., Dasgupta, D., Chakrabarti, P., Roy, S., & Das, C. (2020). A novel role of tumor suppressor ZMYND8 in inducing differentiation of breast cancer cells through its dual-histone binding function. *Journal of Biosciences*, *45*(1), 2. https://doi.org/10.1007/s12038-019-9980-5
Nagai, Y., Miyazawa, H., Huqun, null, Tanaka, T., Udagawa, K., Kato, M., Fukuyama, S., Yokote, A., Kobayashi, K., Kanazawa, M., & Hagiwara, K. (2005). Genetic heterogeneity of the epidermal growth factor receptor in non-small cell lung cancer cell lines revealed by a rapid and sensitive detection system, the peptide nucleic acid-locked nucleic acid PCR clamp. *Cancer Research*, *65*(16), 7276–7282. https://doi.org/10.1158/0008-5472.CAN-05-0331
Navarrete-Perea, J., Yu, Q., Gygi, S. P., & Paulo, J. A. (2018). Streamlined Tandem Mass Tag (SL-TMT) Protocol: An Efficient Strategy for Quantitative (Phospho)proteome Profiling Using Tandem Mass Tag-Synchronous Precursor Selection-MS3. *Journal of Proteome Research*, *17*(6), 2226–2236. https://doi.org/10.1021/acs.jproteome.8b00217
Nusinow, D. P., Szpyt, J., Ghandi, M., Rose, C. M., McDonald, E. R., Kalocsay, M., Jané-Valbuena, J., Gelfand, E., Schweppe, D. K., Jedrychowski, M., Golji, J., Porter, D. A., Rejtar, T., Wang, Y. K., Kryukov, G. V., Stegmeier, F., Erickson, B. K., Garraway, L. A., Sellers, W. R., & Gygi, S. P. (2020). Quantitative Proteomics of the Cancer Cell Line Encyclopedia. *Cell*, *180*(2), 387-402.e16. https://doi.org/10.1016/j.cell.2019.12.023
Oehme, I., Deubzer, H. E., Wegener, D., Pickert, D., Linke, J.-P., Hero, B., Kopp-Schneider, A., Westermann, F., Ulrich, S. M., von Deimling, A., Fischer, M., & Witt, O. (2008). Histone Deacetylase 8 in Neuroblastoma Tumorigenesis. *Clinical Cancer Research*, *15*(1), 91–99. https://doi.org/10.1158/1078-0432.CCR-08-0684
Ogawa, H., Ishiguro, K.-I., Gaubatz, S., Livingston, D. M., & Nakatani, Y. (2002). A complex with chromatin modifiers that occupies E2F- and Myc-responsive genes in G0 cells. *Science (New York, N.Y.)*, *296*(5570), 1132–1136. https://doi.org/10.1126/science.1069861
Okabe, T., Okamoto, I., Tamura, K., Terashima, M., Yoshida, T., Satoh, T., Takada, M., Fukuoka, M., & Nakagawa, K. (2007). Differential constitutive activation of the epidermal growth factor receptor in non-small cell lung cancer cells bearing EGFR gene mutation and amplification. *Cancer Research*, *67*(5), 2046–2053. https://doi.org/10.1158/0008-5472.CAN-06-3339
Osada, H., Tatematsu, Y., Saito, H., Yatabe, Y., Mitsudomi, T., & Takahashi, T. (2004). Reduced expression of class II histone deacetylase genes

is associated with poor prognosis in lung cancer patients. *International Journal of Cancer*, *112*(1), 26–32. https://doi.org/10.1002/ijc.20395

Pal, M., Moffa, A., Sreekumar, A., Ethier, S. P., Barder, T. J., Chinnaiyan, A., & Lubman, D. M. (2006). Differential Phosphoprotein Mapping in Cancer Cells Using Protein Microarrays Produced from 2-D Liquid Fractionation. *Analytical Chemistry*, *78*(3), 702–710. https://doi.org/10.1021/ac0511243

Papavassiliou, A. G., & Musti, A. M. (2020). The Multifaceted Output of c-Jun Biological Activity: Focus at the Junction of CD8 T Cell Activation and Exhaustion. *Cells*, *9*(11), 2470. https://doi.org/10.3390/cells9112470

Pascual, M., & Guerri, C. (2007). The peptide NAP promotes neuronal growth and differentiation through extracellular signal-regulated protein kinase and Akt pathways, and protects neurons co-cultured with astrocytes damaged by ethanol. *Journal of Neurochemistry*, *103*(2), 557–568. https://doi.org/10.1111/j.1471-4159.2007.04761.x

Poll, B. G., Leo, K. T., Deshpande, V., Jayatissa, N., Pisitkun, T., Park, E., Yang, C.-R., Raghuram, V., & Knepper, M. A. (2024). A resource database for protein kinase substrate sequence-preference motifs based on large-scale mass spectrometry data. *Cell Communication and Signaling : CCS*, *22*, 137. https://doi.org/10.1186/s12964-023-01436-2

Qiu, X., Mao, Q., Tang, Y., Wang, L., Chawla, R., Pliner, H. A., & Trapnell, C. (2017). Reversed graph embedding resolves complex single-cell trajectories. *Nature Methods*, *14*(10), 979–982. https://doi.org/10.1038/nmeth.4402

Rad, R., Li, J., Mintseris, J., O'Connell, J., Gygi, S. P., & Schweppe, D. K. (2021). Improved Monoisotopic Mass Estimation for Deeper Proteome Coverage. *Journal of Proteome Research*, *20*(1), 591–598. https://doi.org/10.1021/acs.jproteome.0c00563

Raghavan, S. (2022). How inclusive are cell lines in preclinical engineered cancer models? *Disease Models & Mechanisms*, *15*(5), dmm049520. https://doi.org/10.1242/dmm.049520

Raingeaud, J., Whitmarsh, A. J., Barrett, T., Dérijard, B., & Davis, R. J. (1996). MKK3- and MKK6-Regulated Gene Expression Is Mediated by the p38 Mitogen-Activated Protein Kinase Signal Transduction Pathway. *Molecular and Cellular Biology*, *16*(3), 1247–1255. https://doi.org/10.1128/MCB.16.3.1247

Rangel, R., Guzman-Rojas, L., Kodama, T., Kodama, M., Newberg, J. Y., Copeland, N. G., & Jenkins, N. A. (2017). Identification of New Tumor Suppressor Genes in Triple-Negative Breast Cancer. *Cancer Research*, *77*(15), 4089–4101. https://doi.org/10.1158/0008-5472.CAN-17-0785

Reid, T., Valone, F., Lipera, W., Irwin, D., Paroly, W., Natale, R., Sreedharan, S., Keer, H., Lum, B., Scappaticci, F., & Bhatnagar, A. (2004). Phase II trial of the histone deacetylase inhibitor pivaloyloxymethyl butyrate (Pivanex, AN-9) in advanced non-small cell lung cancer. *Lung Cancer*, *45*(3), 381–386. https://doi.org/10.1016/j.lungcan.2004.03.002

Richardson, P. G., Laubach, J. P., Lonial, S., Moreau, P., Yoon, S.-S., Hungria, V. T., Dimopoulos, M. A., Beksac, M., Alsina, M., & San-Miguel, J. F. (2015). Panobinostat: A novel pan-deacetylase inhibitor for the treatment of relapsed or relapsed and refractory multiple myeloma. *Expert Review of Anticancer Therapy*, *15*(7), 737–748. https://doi.org/10.1586/14737140.2015.1047770

Richon, V. M., Sandhoff, T. W., Rifkind, R. A., & Marks, P. A. (2000). Histone deacetylase inhibitor selectively induces p21WAF1 expression and gene-associated histone acetylation. *Proceedings of the National Academy of Sciences*, *97*(18), 10014–10019. https://doi.org/10.1073/pnas.180316197

Richon, V. M., Webb, Y., Merger, R., Sheppard, T., Jursic, B., Ngo, L., Civoli, F., Breslow, R., Rifkind, R. A., & Marks, P. A. (1996). Second generation hybrid polar compounds are potent inducers of transformed cell differentiation. *Proceedings of the National Academy of Sciences of the United States of America*, *93*(12), 5705–5708.

Roboti, P., & High, S. (2012). The oligosaccharyltransferase subunits OST48, DAD1 and KCP2 function as ubiquitous and selective modulators of mammalian N-glycosylation. *Journal of Cell Science*, *125*(14), 3474–3484. https://doi.org/10.1242/jcs.103952

Sanna, M. D., & Galeotti, N. (2018). The HDAC1/c-JUN complex is essential in the promotion of nerve injury-induced neuropathic pain through JNK signaling. *European Journal of Pharmacology*, *825*, 99–106. https://doi.org/10.1016/j.ejphar.2018.02.034

Sawai, C. M., Freund, J., Oh, P., Ndiaye-Lobry, D., Bretz, J. C., Strikoudis, A., Genesca, L., Trimarchi, T., Kelliher, M. A., Clark, M., Soulier, J., Chen-Kiang, S., & Aifantis, I. (2012). Therapeutic Targeting of the Cyclin D3:CDK4/6 Complex in T Cell Leukemia. *Cancer Cell*, *22*(4), 452–465. https://doi.org/10.1016/j.ccr.2012.09.016

Schrump, D. S., Fischette, M. R., Nguyen, D. M., Zhao, M., Li, X., Kunst, T. F., Hancox, A., Hong, J. A., Chen, G. A., Kruchin, E., Wright, J. J., Rosing, D. R., Sparreboom, A., Figg, W. D., & Steinberg, S. M. (2008). Clinical and Molecular Responses in Lung Cancer Patients Receiving Romidepsin. *Clinical Cancer Research*, *14*(1), 188–198. https://doi.org/10.1158/1078-0432.CCR-07-0135

Schweppe, D. K., Eng, J. K., Yu, Q., Bailey, D., Rad, R., Navarrete-Perea, J., Huttlin, E. L., Erickson, B. K., Paulo, J. A., & Gygi, S. P. (2020). Full-Featured, Real-Time Database Searching Platform Enables Fast and Accurate Multiplexed Quantitative Proteomics. *Journal of Proteome Research*, *19*(5), 2026–2034. https://doi.org/10.1021/acs.jproteome.9b00860

Schweppe, D. K., Huttlin, E. L., Harper, J. W., & Gygi, S. P. (2018). BioPlex Display: An Interactive Suite for Large-Scale AP–MS Protein–Protein Interaction Data. *Journal of Proteome Research*, *17*(1), 722–726. https://doi.org/10.1021/acs.jproteome.7b00572

Schweppe, D. K., Rigas, J. R., & Gerber, S. A. (2013). Quantitative phosphoproteomic profiling of human non-small cell lung cancer tumors. *Journal of Proteomics*, *91*, 286–296. https://doi.org/10.1016/j.jprot.2013.07.023

Searfoss, R. M., Karki, R., Lin, Z., Robison, F., & Garcia, B. A. (2023). An Optimized and High-Throughput Method for Histone Propionylation and Data-Independent Acquisition Analysis for the Identification and Quantification of Histone Post-translational Modifications. *Journal of the American Society for Mass Spectrometry*, *34*(11), 2508–2517. https://doi.org/10.1021/jasms.3c00223

Seto, E., & Yoshida, M. (2014). Erasers of Histone Acetylation: The Histone Deacetylase Enzymes. *Cold Spring Harbor Perspectives in Biology*, *6*(4), a018713. https://doi.org/10.1101/cshperspect.a018713

Shanmugam, G., Rakshit, S., & Sarkar, K. (2022). HDAC inhibitors: Targets for tumor therapy, immune modulation and lung diseases. *Translational Oncology*, *16*, 101312. https://doi.org/10.1016/j.tranon.2021.101312

Shannon, P., Markiel, A., Ozier, O., Baliga, N. S., Wang, J. T., Ramage, D., Amin, N., Schwikowski, B., & Ideker, T. (2003). Cytoscape: A software environment for integrated models of biomolecular interaction networks. *Genome Research*, *13*(11), 2498–2504. https://doi.org/10.1101/gr.1239303

Shin, D., Park, J., Han, D., Moon, J. H., Ryu, H. S., & Kim, Y. (2020). Identification of TUBB2A by quantitative proteomic analysis as a novel biomarker for the prediction of distant metastatic breast cancer. *Clinical Proteomics*, *17*(1), 16. https://doi.org/10.1186/s12014-020-09280-z

Shulak, L., Beljanski, V., Chiang, C., Dutta, S. M., Van Grevenynghe, J., Belgnaoui, S. M., Nguyên, T. L.-A., Di Lenardo, T., Semmes, O. J., Lin, R., & Hiscott, J. (2014). Histone Deacetylase Inhibitors Potentiate Vesicular Stomatitis Virus Oncolysis in Prostate Cancer Cells by Modulating NF-κB-Dependent Autophagy. *Journal of Virology*, *88*(5), 2927–2940. https://doi.org/10.1128/jvi.03406-13

Siavoshian, S., Segain, J.-P., Kornprobst, M., Bonnet, C., Cherbut, C., Galmiche, J.-P., & Blottière, H. M. (2000). Butyrate and trichostatin A effects on the proliferation/differentiation of human intestinal epithelial cells: Induction of cyclin D3 and p21 expression. *Gut*, *46*(4), 507–514. https://doi.org/10.1136/gut.46.4.507

Sidoli, S., Bhanu, N. V., Karch, K. R., Wang, X., & Garcia, B. A. (2016). Complete Workflow for Analysis of Histone Post-translational Modifications Using Bottom-up Mass Spectrometry: From Histone Extraction to Data Analysis. *Journal of Visualized Experiments: JoVE*, *111*, 54112. https://doi.org/10.3791/54112

Smith, S. L., Bowers, N. L., Betticher, D. C., Gautschi, O., Ratschiller, D., Hoban, P. R., Booton, R., Santibáñez-Koref, M. F., & Heighway, J. (2005). Overexpression of aurora B kinase (AURKB) in primary non-small cell lung carcinoma is frequent, generally driven from one allele, and correlates with the level of genetic instability. *British Journal of Cancer*, *93*(6), 719–729. https://doi.org/10.1038/sj.bjc.6602779

Srivatsan, S. R., McFaline-Figueroa, J. L., Ramani, V., Saunders, L., Cao, J., Packer, J., Pliner, H. A., Jackson, D. L., Daza, R. M., Christiansen, L., Zhang, F., Steemers, F., Shendure, J., & Trapnell, C. (2020). Massively multiplex chemical transcriptomics at single-cell resolution. *Science*, *367*(6473), 45–51. https://doi.org/10.1126/science.aax6234

Sudo, T., Mimori, K., Nishida, N., Kogo, R., Iwaya, T., Tanaka, F., Shibata, K., Fujita, H., Shirouzu, K., & Mori, M. (2011). Histone deacetylase 1 expression in gastric cancer. *Oncology Reports*, *26*(4), 777–782. https://doi.org/10.3892/or.2011.1361

Sugimoto, A., Hozak, R. R., Nakashima, T., Nishimoto, T., & Rothman, J. H. (1995). Dad-1, an endogenous programmed cell death suppressor in Caenorhabditis elegans and vertebrates. *The EMBO Journal*, *14*(18), 4434–4441. https://doi.org/10.1002/j.1460-2075.1995.tb00122.x

Sugiyama, N., Imamura, H., & Ishihama, Y. (2019). Large-scale Discovery of Substrates of the Human Kinome. *Scientific Reports*, *9*(1), 10503. https://doi.org/10.1038/s41598-019-46385-4

Takahashi, Y., Tanikawa, C., Miyamoto, T., Hirata, M., Wang, G., Ueda, K., Komatsu, T., & Matsuda, K. (2017). Regulation of tubular recycling endosome biogenesis by the p53-MICALL1 pathway. *International Journal of Oncology*, *51*(2), 724–736. https://doi.org/10.3892/ijo.2017.4060

Teye, K., Tsuneoka, M., Arima, N., Koda, Y., Nakamura, Y., Ueta, Y., Shirouzu, K., & Kimura, H. (2004). Increased Expression of a Myc Target Gene Mina53 in Human Colon Cancer. *The American Journal of Pathology*, *164*(1), 205–216.

Tharkar-Promod, S., Johnson, D. P., Bennett, S. E., Dennis, E. M., Banowsky, B. G., Jones, S. S., Shearstone, J. R., Quayle, S. N., Min, C., Jarpe, M., Mosbruger, T., Pomicter, A. D., Miles, R. R., Chen, W. Y., Bhalla, K. N., Zweidler-McKay, P. A., Shrieve, D. C., Deininger, M. W., Chandrasekharan, M. B., & Bhaskara, S. (2018). HDAC1,2 inhibition and doxorubicin impair Mre11-dependent DNA repair and DISC to override BCR-ABL1-driven DSB repair in Philadelphia chromosome-positive B-cell precursor acute lymphoblastic leukemia. *Leukemia*, *32*(1), 49–60. https://doi.org/10.1038/leu.2017.174

Trapnell, C., Cacchiarelli, D., Grimsby, J., Pokharel, P., Li, S., Morse, M., Lennon, N. J., Livak, K. J., Mikkelsen, T. S., & Rinn, J. L. (2014). The dynamics and regulators of cell fate decisions are revealed by pseudotemporal ordering of single cells. *Nature Biotechnology*, *32*(4), 381–386. https://doi.org/10.1038/nbt.2859

Traynor, A. M., Dubey, S., Eickhoff, J. C., Kolesar, J. M., Schell, K., Huie, M. S., Groteluschen, D. L., Marcotte, S. M., Hallahan, C. M., Weeks, H. R., Wilding, G., Espinoza-Delgado, I., & Schiller, J. H. (2009). Vorinostat (NSC# 701852) in Patients with Relapsed Non-small Cell Lung Cancer: A Wisconsin Oncology Network Phase II Study. *Journal of Thoracic Oncology*, *4*(4), 522–526. https://doi.org/10.1097/JTO.0b013e3181952478

Tsuchida, N., Ikeda, M.-A., Ishino, Y., Grieco, M., & Vecchio, G. (2017). FUCA1 is induced by wild-type p53 and expressed at different levels in thyroid cancers depending on p53 status Corrigendum in /10.3892/ijo.2017.4077. *International Journal of Oncology*, *50*(6), 2043–2048. https://doi.org/10.3892/ijo.2017.3968

Uhlen, M., Zhang, C., Lee, S., Sjöstedt, E., Fagerberg, L., Bidkhori, G., Benfeitas, R., Arif, M., Liu, Z., Edfors, F., Sanli, K., Von Feilitzen, K., Oksvold, P., Lundberg, E., Hober, S., Nilsson, P., Mattsson, J., Schwenk, J. M., Brunnström, H., … Ponten, F. (2017). A pathology atlas of the human cancer transcriptome. *Science*, *357*(6352), eaan2507. https://doi.org/10.1126/science.aan2507

Valeria, P. de L., & Raúl, B.-R. (2005). Changes in P-glycoprotein activity are mediated by the growth of a tumour cell line as multicellular spheroids. *Cancer Cell International*, *5*(1), 20. https://doi.org/10.1186/1475-2867-5-20

Van Vranken, J. G., Li, J., Mintseris, J., Gadzuk-Shea, M., Gygi, S. P., & Schweppe, D. K. (2024). Large-scale characterization of drug mechanism of action using proteome-wide thermal shift assays. *bioRxiv*, 2024.01.26.577428. https://doi.org/10.1101/2024.01.26.577428

Van Vranken, J. G., Li, J., Mitchell, D. C., Navarrete-Perea, J., & Gygi, S. P. (2021). Assessing target engagement using proteome-wide solvent shift assays. *eLife*, *10*, e70784. https://doi.org/10.7554/eLife.70784

Vrana, J. A., Decker, R. H., Johnson, C. R., Wang, Z., Jarvis, W. D., Richon, V. M., Ehinger, M., Fisher, P. B., & Grant, S. (1999). Induction of apoptosis in U937 human leukemia cells by suberoylanilide hydroxamic acid (SAHA) proceeds through pathways that are regulated by Bcl-2/Bcl-XL, c-Jun, and p21CIP1, but independent of p53. *Oncogene*, *18*(50), Article 50. https://doi.org/10.1038/sj.onc.1203176

Wang, D., Eraslan, B., Wieland, T., Hallström, B., Hopf, T., Zolg, D. P., Zecha, J., Asplund, A., Li, L., Meng, C., Frejno, M., Schmidt, T., Schnatbaum, K., Wilhelm, M., Ponten, F., Uhlen, M., Gagneur, J., Hahne, H., & Kuster, B. (2019). A deep proteome and transcriptome abundance atlas of 29 healthy human tissues. *Molecular Systems Biology*, *15*(2), e8503. https://doi.org/10.15252/msb.20188503

Weichert, W., Denkert, C., Noske, A., Darb-Esfahani, S., Dietel, M., Kalloger, S. E., Huntsman, D. G., & Köbel, M. (2008). Expression of Class I Histone Deacetylases Indicates Poor Prognosis in Endometrioid Subtypes of Ovarian and Endometrial Carcinomas. *Neoplasia*, *10*(9), 1021–1027. https://doi.org/10.1593/neo.08474

Weichert, W., Röske, A., Gekeler, V., Beckers, T., Ebert, M. P., Pross, M., Dietel, M., Denkert, C., & Röcken, C. (2008). Association of patterns of class I histone deacetylase expression with patient prognosis in gastric cancer: A retrospective analysis. *The Lancet Oncology*, *9*(2), 139–148. https://doi.org/10.1016/S1470-2045(08)70004-4

Witta, S. (2012). Histone Deacetylase Inhibitors in Non–Small-Cell Lung Cancer. *Journal of Thoracic Oncology*, *7*(12), S404–S406. https://doi.org/10.1097/JTO.0b013e31826df29c

Wu, L., Wang, Y., Liu, Y., Yu, S., Xie, H., Shi, X., Qin, S., Ma, F., Tan, T. Z., Thiery, J. P., & Chen, L. (2014). A central role for TRPS1 in the control of cell cycle and cancer development. *Oncotarget*, *5*(17), 7677–7690.

Xiao, H., Hasegawa, T., & Isobe, K. (1999). Both Sp1 and Sp3 are responsible for p21waf1 promoter activity induced by histone deacetylase inhibitor in NIH3T3 cells. *Journal of Cellular Biochemistry*, *73*(3), 291–302. https://doi.org/10.1002/(SICI)1097-4644(19990601)73:3<291::AID-JCB1>3.0.CO;2-5

Yang, Y., Yin, L., Zhu, M., Song, S., Sun, C., Han, X., Xu, Y., Zhao, Y., Qi, Y., Xu, L., & Peng, J.-Y. (2021). Protective effects of dioscin on

vascular remodeling in pulmonary arterial hypertension via adjusting GRB2/ERK/PI3K-AKT signal. *Biomedicine & Pharmacotherapy*, *133*, 111056. https://doi.org/10.1016/j.biopha.2020.111056

Yuan, Z.-F., Lin, S., Molden, R. C., Cao, X.-J., Bhanu, N. V., Wang, X., Sidoli, S., Liu, S., & Garcia, B. A. (2015). EpiProfile Quantifies Histone Peptides With Modifications by Extracting Retention Time and Intensity in High-resolution Mass Spectra*,. *Molecular & Cellular Proteomics*, *14*(6), 1696–1707. https://doi.org/10.1074/mcp.M114.046011

Zamostiano, R., Pinhasov, A., Gelber, E., Steingart, R. A., Seroussi, E., Giladi, E., Bassan, M., Wollman, Y., Eyre, H. J., Mulley, J. C., Brenneman, D. E., & Gozes, I. (2001). Cloning and Characterization of the Human Activity-dependent Neuroprotective Protein*. *Journal of Biological Chemistry*, *276*(1), 708–714. https://doi.org/10.1074/jbc.M007416200

Zhang, J., Kalyankrishna, S., Wislez, M., Thilaganathan, N., Saigal, B., Wei, W., Ma, L., Wistuba, I. I., Johnson, F. M., & Kurie, J. M. (2007). Src-Family Kinases Are Activated in Non-Small Cell Lung Cancer and Promote the Survival of Epidermal Growth Factor Receptor-Dependent Cell Lines. *The American Journal of Pathology*, *170*(1), 366–376. https://doi.org/10.2353/ajpath.2007.060706

Zhang, Q., Thakur, C., Fu, Y., Bi, Z., Wadgaonkar, P., Xu, L., Liu, Z., Liu, W., Wang, J., Kidder, B. L., & Chen, F. (2020). Mdig promotes oncogenic gene expression through antagonizing repressive histone methylation markers. *Theranostics*, *10*(2), 602–614. https://doi.org/10.7150/thno.36220

Zhang, Y., Lu, Y., Yuan, B.-Z., Castranova, V., Shi, X., Stauffer, J. L., Demers, L. M., & Chen, F. (2005). The Human mineral dust-induced gene, mdig, is a cell growth regulating gene associated with lung cancer. *Oncogene*, *24*(31), Article 31. https://doi.org/10.1038/sj.onc.1208668

Zhao, T., Kee, H. J., Bai, L., Kim, M.-K., Kee, S.-J., & Jeong, M. H. (2021). Selective HDAC8 Inhibition Attenuates Isoproterenol-Induced Cardiac Hypertrophy and Fibrosis via p38 MAPK Pathway. *Frontiers in Pharmacology*, *12*. https://www.frontiersin.org/articles/10.3389/fphar.2021.677757

Zhou, F., & Zhou, C. (2018). Lung cancer in never smokers—The East Asian experience. *Translational Lung Cancer Research*, *7*(4). https://doi.org/10.21037/tlcr.2018.05.14

Zhou, M., Liu, H., Xu, X., Zhou, H., Li, X., Peng, C., Shen, S., Xiong, W., Ma, J., Zeng, Z., Fang, S., Nie, X., Yang, Y., Zhou, J., Xiang, J., Cao, L., Peng, S., Li, S., & Li, G. (2006). Identification of nuclear localization signal that governs nuclear import of BRD7 and its essential roles in inhibiting cell cycle progression. *Journal of Cellular Biochemistry*, *98*(4), 920–930. https://doi.org/10.1002/jcb.20788

Zhu, S., Xu, Z., Zeng, Y., Long, Y., Fan, G., Ding, Q., Wen, Y., Cao, J., Dai, T., Han, W., & Xie, Y. (2020). ADNP Upregulation Promotes Bladder Cancer Cell Proliferation via the AKT Pathway. *Frontiers in Oncology*, *10*. https://www.frontiersin.org/articles/10.3389/fonc.2020.491129